

DRAFT

**BULKING FACTOR OF ROCK FOR
UNDERGROUND OPENINGS**

Prepared for

**U.S. Nuclear Regulatory Commission
Contract NRC 02-07-006**

Prepared by

**Goodluck I. Ofoegbu¹
Rodney S. Read²
Fernando Ferrante¹**

**¹Center for Nuclear Waste Regulatory Analyses
San Antonio, Texas**

**²RSRead Consulting, Inc.
Okotoks, Alberta, Canada**

February 2008

DRAFT

DRAFT

ABSTRACT

This report presents the results of a literature review, field work, and laboratory testing to examine ways of characterizing the bulking of rock when it breaks up to form rubble. Field and laboratory work that Center for Nuclear Waste Regulatory Analyses and U.S. Nuclear Regulatory Commission staffs performed to obtain information relevant to assessing bulking factors is also described. The information reviewed includes data from (i) underground excavations near Yucca Mountain, (ii) surface excavation of rock and soil, and (iii) underground mining. The review resulted in a compilation of bulking factor data from various sources, representing a wider range of conditions than could be expected for a degraded emplacement drift at a potential Yucca Mountain repository. The data was statistically analyzed using techniques for summarizing expert opinions. The bulking factor distribution used for staff analysis of drift degradation effects on repository performance may need to be updated to be consistent with information discussed in the report.

DRAFT

CONTENTS

Section	Page
ABSTRACT	ii
FIGURES	iv
TABLES	v
ACKNOWLEDGMENTS	vi
EXECUTIVE SUMMARY	vii
1 INTRODUCTION.....	1-1
2 LITERATURE REVIEW.....	2-1
2.1 DOE Information on Bulking Factor.....	2-1
2.2 Bulking Factor in Surface Excavation.....	2-6
2.3 Bulking Factor in Underground Mining.....	2-7
2.3.1 Hard Rock Mining	2-7
2.3.2 Caving Methods of Mining	2-9
2.3.3 Underground Coal Mining.....	2-10
2.4 Measurement of Bulking Factor.....	2-18
3 SUMMARY OF BULKING FACTOR INFORMATION	3-1
4 CONCLUSIONS	4-1
5 REFERENCES.....	5-1
APPENDIX A—ESTIMATED BULKING FACTORS FOR GEOLOGIC MATERIALS	
APPENDIX B—SUMMARY OF FRACTURE AND RUBBLE CHARACTERIZATION FROM LITHOPHYSAL TUFF AT THE SOUTH END OF FRAN RIDGE, YUCCA MOUNTAIN, NEVADA	
APPENDIX C—LABORATORY MEASUREMENT OF BULKING FACTOR	

DRAFT

FIGURES

Figure		Page
2-1	Range of Degraded Drift Shapes	2-1
2-2	Relations Between Normalized Cave Height and Bulking Factor for a Range of Friction Angle (ϕ or ϕ) Values	2-2
2-3	Schematic Illustrating the Effect of Fall Height on Void Space Between Gob Fragments	2-11
2-4	Relation Between Ratio of Fall Height to Block Width (H/B) and Bulking Factor for Longwall Coal Gob.....	2-12
2-5	Relation Between Overburden Stress and Bulking Factor for a Range of Unconfined Compressive Strength (UCS) and Thickness-to-Width Ratios (T/W).....	2-15
3-1	Range of Bulking Factor Probability Density Functions for the Subset of 16, Where Each Individual Input Is Represented by a Uniform Probability.....	3-12
3-2	Aggregate (A) Probability Density $f(B)$ and (B) Cumulative Distribution $F(B)$ for the Subset of 16 Shown in Figure 3-1 Resulting From a Linear Weighted Average	3-13
3-3	Range of Bulking Factor Probability Density Functions for the Subset of 16, Where Each Individual Input Is Represented by a Normal Probability Density.....	3-15
3-4	Aggregate (A) Probability Density $f(B)$ and (B) Cumulative Distribution $F(B)$ for the Subset of 16 Shown in Figure 3-1 Resulting From a Linear Weighted Average.....	3-16
3-5	Comparison Between the Bulking Factor Probability Densities for the Input Distribution Currently Assumed in the TPA Code and the Aggregate Distribution.....	3-17

DRAFT

TABLES

Table		Page
2-1	Typical Bulking Factor Values for Surface Excavation.....	2-7
2-2	Typical Bulking Factors for Mined Rock.....	2-8
2-3	Derived Parameters Relating Bulking Factor to Rock Strength and Shape Ratio.....	2-14
2-4	Coefficients for Average Caving Height and Predicted Bulking Factors for Chinese Coal Mines	2-16
2-5	Bulking Factors for South African Coal Measure Rocks	2-18
2-6	Bulking Factors for Coal Measure Rocks.....	2-18
3-1	Summary of Bulking Factor Information From Literature	3-2
3-2	Bulking Factor Distribution Derived From the Subset of 16 Literature Data in Table 3-1 Assuming a Beta Distribution Fit.....	3-17

DRAFT

ACKNOWLEDGMENTS

This report was prepared to document work performed by the Center for Nuclear Waste Regulatory Analyses (CNWRA) for the U.S. Nuclear Regulatory Commission (US NRC) under Contract No. NRC-02-07-006. The activities reported here were performed on behalf of the US NRC Office of Nuclear Material Safety and Safeguards, Division of High-Level Waste Repository Safety. The report is an independent product of CNWRA and does not necessarily reflect the views or regulatory position of NRC.

The authors are grateful to Arturo Ramos, Lauren Mulverhill, Asad Chowdhury, Wesley Patrick, and Sitakanta Mohanty for reviews and document preparation assistance. Danielle Wyrick,¹ Kevin Smart,¹ Randall Fedors,² and Ronald McGinnis¹ prepared Appendix B to document rubble characterization field studies at Fran Ridge. Robert Lenhard,¹ Chandrika Manepally,¹ and Donald Bannon¹ prepared Appendix C to document laboratory studies on Fran Ridge rubble samples.

QUALITY OF DATA, ANALYSES, AND CODE DEVELOPMENT

DATA: All CNWRA-generated data contained in this report meet quality assurance requirements described in the Geosciences and Engineering Division Quality Assurance Manual and are documented in CNWRA Scientific Notebooks 779E and 852E. Sources of other data should be consulted for determining the level of quality of those data.

ANALYSES AND CODES: MATLAB (Version 7.1.0.246 R14 Service Pack3, License Number 301039), a general purpose programming environment developed by MathWorks, Inc. (2005), was used to perform the statistical analysis calculations. Microsoft® Excel® (Version 2002) (Microsoft Corporation, Inc., 2002) and Rockware StereoStat® (Version 1.4) (Rockware, Inc., 2004) were also used for analysis. MATLAB, MICROSOFT EXCEL, and ROCKWARE STEREO STAT are exempt off-the-shelf commercial software as defined in the quality assurance procedure Technical Operating Procedure—018, Development and Control of Scientific and Engineering Software (Geosciences and Engineering Division, 2005). Several supporting analyses for the report are documented in CNWRA Scientific Notebook 918E.

REFERENCES

Geosciences and Engineering Division. "Quality Assurance Manual." San Antonio, Texas: Geosciences and Engineering Division. 2005.

Mathworks, Inc. "MATLAB User's Manual." Version 7.1.0. Natick, Massachusetts: Mathworks, Inc. 2005.

Microsoft Corporation, Inc. "Microsoft Excel 2002." Redmond, Washington: Microsoft Corporation. 2002.

Rockware, Inc. "Stereo Stat Version 1.4." Golden, Colorado: Rockware, Inc. 2004.

¹Center for Nuclear Waste Regulatory Analyses; San Antonio, Texas

² U.S. Nuclear Regulatory Commission; Washington, DC

DRAFT

EXECUTIVE SUMMARY

The bulking factor parameter is used to describe an increase in volume that may occur when a block of rock breaks up to form rubble or when a mass of soil is excavated. Staff expects to use the parameter to estimate the extent of any drift degradation and volume of rubble that may accumulate in degraded drifts, and for thermal-hydrological evaluations of rubble effects, if the emplacement drifts degraded after permanent closure of a potential repository at Yucca Mountain (CNWRA, 2007). This report summarizes bulking factor information from the literature, assesses the relevance of the information for estimating potential rubble accumulations in emplacement drifts in welded tuff, and presents information from field and laboratory studies that may assist understanding the bulking behavior of Yucca Mountain welded tuff. The literature review considered published bulking factor information from (i) underground excavations near Yucca Mountain including the Nevada Test Site; (ii) surface excavation of rock and soil, including placer mining and civil works; and (iii) underground mining, particularly hard rock mining and special application of caving and longwall methods of ore extraction. Examples of bulking factor values were identified from each of these engineering areas. In most cases, the original authors did not explicitly define the method used to determine the cited values. Therefore, any uncertainties in these values that may arise from the measurement procedure were not defined.

Bulking factor information was also collected through analysis of field data from Fran Ridge, near Yucca Mountain, and laboratory testing of rubble specimens. The field data includes plots of rubble shape and size distributions that could be used to estimate bulking factors. However, the field data has not been used to determine bulking factors, because the relationships between bulking factor and the size and shape distributions of rubble particles are not well understood. Therefore, the field data were not included in the aggregation of bulking factor data presented in this report.

The literature and laboratory data (including data from laboratory test results in Appendix C) were statistically analyzed using techniques developed for summarizing expert opinions to obtain a distribution function for bulking factor. The calculated bulking factor distribution has a mean of 38.4 percent, a standard deviation of 19.6 percent, and the following probability density areas.

The distribution was calculated using a subset of the data the authors considered to represent rock types and rubble mechanisms relevant to welded volcanic tuff. The distribution represents a wider range of conditions than could be expected for a degraded emplacement drift at a potential Yucca Mountain repository. The Total-system Performance Assessment Version 5.1a input parameters representing bulking factor (CNWRA, 2007) may need to be updated to be consistent with the distribution developed in this report.

Bulking Factor, B (Percentage)	Corresponding TPA 5.1a Bulking Factor, B₁	Probability Density Area (Percentage)
B < 10%	B ₁ < 1.1	6.0
10% < B < 60%	1.1 < B ₁ < 1.6	78.4
10% < B < 90%	1.1 < B ₁ < 1.9	93.8
B < 90%	B ₁ < 1.9	99.7
Mean bulking factor = 38.4 percent, standard deviation = 19.6 percent Mean of B ₁ = 1.38, standard deviation = 0.196 Beta distribution parameters: α = 1.97, β = 3.2		

DRAFT

DRAFT

REFERENCES

CNWRA. "Total-system Performance Assessment (TPA) Version 5.1a." San Antonio, Texas: CNWRA. September 2007.

DRAFT

1 INTRODUCTION

Bulking is the phenomenon of volume increase that occurs when solid rock is broken (Nelson, 1965). The volume of broken rock may increase relative to the original volume because the broken rock pieces typically do not fit together perfectly, which results in an increase in void space included with the rock solids. Depending on its initial state of consolidation, bulking also may occur when soil is excavated, resulting in a soil volume greater than the initial volume. The bulking factor B for rock may be defined using the equation

$$B = V_B / V - 1 \quad 1-1$$

where V_B is the volume of rubble formed from breakage of a rock block of initial volume V (e.g., Bechtel SAIC Company, LLC, 2004). Bulking factor also may be specified as a parameter B_1 related to B through the following equation (e.g., Ofoegbu, et al., 2007; CNWRA, 2007)

$$B_1 = 1 + B = V_B / V \quad 1-2$$

Eqs. (1-1) and (1-2) also represent the bulking of excavated soil, wherein V is the *in-situ* volume of the soil and V_B is the volume after excavation. V_B is usually greater than V , but compaction of an excavated soil typically results in a V_B smaller than V .

Bulking factor is used in mining and civil engineering to estimate the volume of materials generated from excavation or collapse of rock surrounding mine openings. Staff expects to use bulking factors to estimate the extent of any drift degradation, volume of rubble that may accumulate in degraded drifts, and thermal-hydrological properties if the emplacement drifts degraded after permanent closure of a potential repository at Yucca Mountain (CNWRA, 2007). Staff will use such estimates to inform its review of any U.S. Department of Energy (DOE) assessments of potential drift degradation, resulting rubble loading of components of the engineered barrier system, and thermal-hydrological effects of rubble.

This report summarizes published information related to bulking factor, emphasizing information relevant to degradation of underground excavations. Available literature information is discussed to explore the effects of rock type, particle size and shape distributions, and other characteristics of rubble and the environment that may affect bulking factor values. Bulking factor data from the literature was statistically analyzed as part of the review to obtain a bulking factor distribution function. Techniques for measurement of bulking factor are also discussed along with rock mass characteristics based on observations of rock outcrops at Yucca Mountain that may be relevant to estimating bulking factor values for Yucca Mountain volcanic tuff. Appendix B describes field work performed to characterize surface exposures at the southern end of Fran Ridge. Data relevant to characterizing fracture and shape and size distribution of rubble fragments were collected and analyzed. Rubble samples collected at Fran Ridge were used in a laboratory experiment described in Appendix C to measure bulking factor.

2 LITERATURE REVIEW

The literature review considered published information on bulking factor in a number of different contexts: underground excavations near Yucca Mountain including information based on work done at the Nevada Test Site; surface excavation of rock and soil, including placer mining and civil works; and underground mining, considering hard rock mining and special application of caving and longwall methods of ore extraction. Examples of bulking factor values were identified for each of these contexts. In several cases, the original authors did not explicitly define the method used to determine the cited values. Therefore, any uncertainties in these values that may arise from the measurement procedure are unknown in such cases. Nonetheless, the literature review highlights the use of bulking factor to estimate the extent of degradation of excavated openings and quantities of rock rubble, indicates ranges of bulking factor values for various conditions, identifies factors that affect bulking factor, and describes different methods for determining bulking factor. A summary of published bulking factor values including a judgment of their relevance for assessing potential drift degradation effects at Yucca Mountain and a statistical analysis of the resulting data are presented in Chapter 3.

2.1 DOE Information on Bulking Factor

Bechtel SAIC Company, LLC (2004) describes the effects of bulking factor on estimates of drift degradation extent and rubble accumulation. The estimates also vary with the assumed degraded-drift shape. Bechtel SAIC Company, LLC (2004) presented calculations for two shapes referred to as the piping (or chimney) and the Terzaghi (or trapezoidal) collapse models. The first model represents drifts that degrade vertically and the second represents drifts that degrade both laterally and vertically. The Terzaghi collapse model is based on an assumption that rock surrounding the drift opening may collapse along slip lines angled at $45 + \phi/2^\circ$ to the vertical and tangent to the drift wall (where ϕ is the friction angle), resulting in a rubble volume of width W and height H above the drift (Figure 2-1).

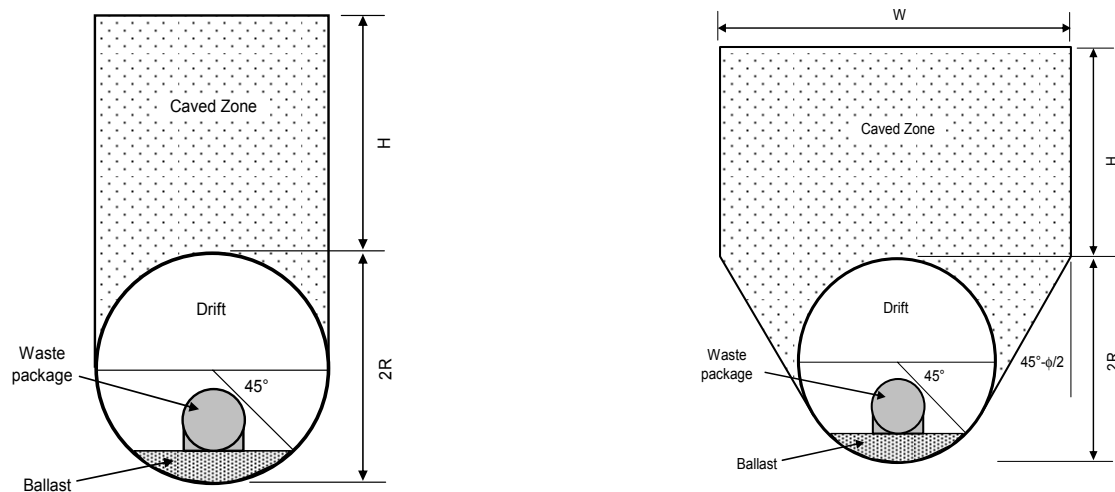


Figure 2-1. Range of Degraded-Drift Shapes (Bechtel SAIC Company, LLC, 2004). The Chimney Collapse Model (Left) Is a Special Case of the More General Terzaghi Collapse Model (Right), Which Considers Friction Angle (ϕ) in the Calculation of Caved Zone Height. R Is the Radius of the Circular Drift.

DRAFT

The degraded-drift height, and therefore the amount of rubble accumulation, can be calculated using the geometry illustrated in Figure 2-1. For bulking factors ranging from 20 to 40 percent, cave heights above the drift ranged from 2.6 to 1.2 times the drift diameter for the chimney model and from 1.8 to 0.9 times the drift diameter for the Terzaghi model (Figure 2-2).

Two members of a DOE-convened six-member expert panel on near-field/altered-zone coupled effects provided opinions on values of bulking factor for Yucca Mountain volcanic tuff (CRWMS M&O, 1998). The panel was tasked with evaluating the temporal and spatial distribution of thermal, hydrologic, mechanical, and chemical effects associated with host rock heating resulting from radioactive wastes disposed underground. The bulking factor opinions of two panel members follow.

Dr. Derek Elsworth:

“Assuming failure of the drift, a bulking factor of about 35 percent may be expected, at the lower end of an anticipated 20 to 65 percent range (Church, 1981), representing drift-infill porosities in the 15 to 40 percent range. In the case of complete failure of the drift by chimneying, this would represent failure to about three diameters above the initial drift, based on geometric constraints alone. This geometric constraint of three diameters provides an approximate upper bound to anticipated drift elongation to about one drift diameter.” (CRWMS M&O, 1998, Section 3.1).

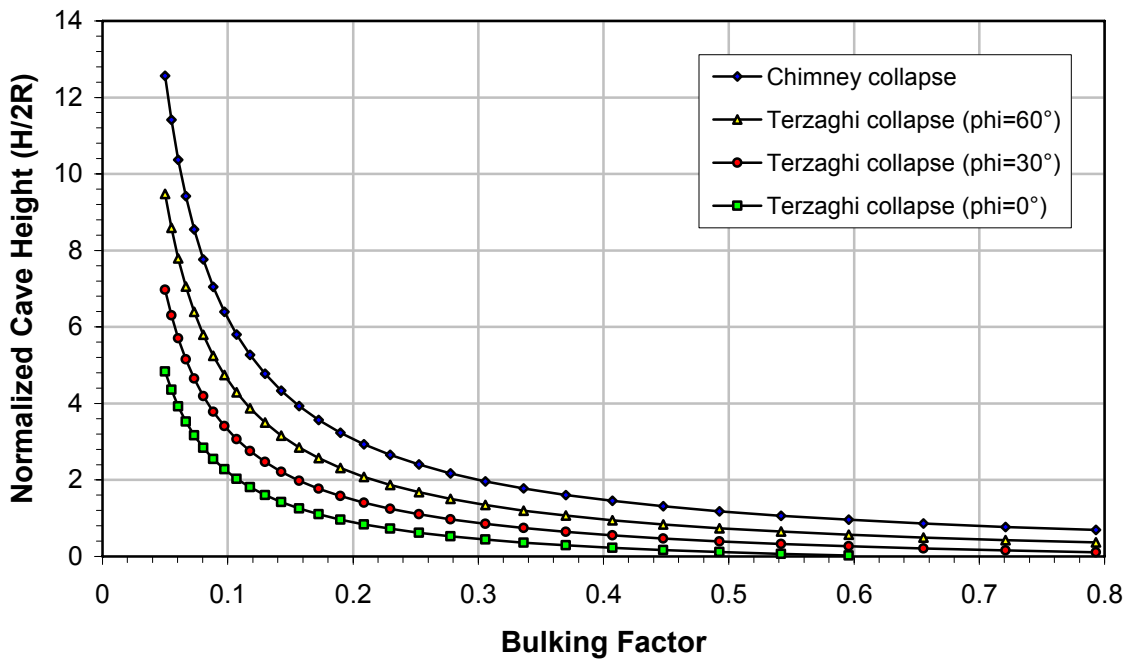


Figure 2-2. Relations Between Normalized Cave Height and Bulking Factor for a Range of Friction Angle (ϕ or ϕ_i) Values. Drift Geometry Parameters H and R Are Defined in Figure 2-1. Minimum Bulking Factor Shown Is 0.05 (i.e., 5 Percent).

DRAFT

Dr. John Gale:

“When the drift fails, the crown will migrate with a bulking factor of about 30 percent (range of 15 to 45 percent), based on the blocky nature of the rock mass. This is equivalent to a porosity of 13 to 31 percent. For a 5-m drift opening, one would expect the crown to migrate 10 to 12 m vertically. There may be some peaking of the ceiling depending on the orientation of local fractures. The crown migration eventually will stop as the back-pressure develops in the caved material.... To help assess the effects of the bulking factor, the work completed by Duncan, et al. (1972), on rubble piles in drifts from blasts at the Nevada Test Site should be reviewed.” (CRWMS M&O, 1998, Section 4.1).

The publication [Church (1981)] cited by Derek Elsworth provides an exhaustive summary of about 1,500 measurements of material characteristics originally published as tables by authoritative sources in the United States dating from 1882. In general, these tables include specific gravity, weight in natural bed, swell factor from the natural bed or cut to the loose condition, weight in the loose condition, swell or shrink factor from the natural bed or cut to fills or compacted embankments, and weight in fills or compacted embankments. For a material such as rock or soil that consists of more than one mineral, the value of specific gravity given in the tables is an apparent (or equivalent) specific gravity (i.e., ratio of material density to density of water). Weight in the natural bed (or bank measurement) includes natural moisture and is equivalent to the *in-situ* bulk density ($\gamma_{in-situ}$). Table A-1 is based on Church (1981), but values for weight have been converted to bulk density in SI units. Percentage swell from the natural bed (or *in-situ* state) to the loose condition is calculated as

$$Swell_i (\%) = 100 \cdot \left(\frac{\gamma_{in-situ}}{\gamma_{loose}} - 1 \right) \quad 2-1$$

where γ_{loose} is unit weight in the loose condition. Percentage swell from *in-situ* to loose condition is equivalent to bulking factor for stockpiled materials under gravity loading.

Church (1981) indicated the bulk densities include an error of up to ± 10 percent, and the swell and shrinkage factors include an error of up to ± 33 percent for both rock and earth materials. Church (1981) assigned a default value of 67 percent to solidly bedded unweathered rocks if no swell factor data was available. For rocks with high porosity, and hence lower *in-situ* bulk density compared to the values contained in Church (1981), the percentage swell from *in-situ* to loose condition may be reduced relative to low porosity rock of the same type assuming the initial pore structure is disrupted (i.e., collapsed) during the bulking process. Additional estimates of bulking factor based on a modified material properties table from Hartman (1992) are also included in Table A-2.

Church (1981) notes that the method of excavation affects swell factor. In considering haulage of material, bulking factors varied considerably between materials excavated with and without blasting. Bulking factors used to estimate the amount of bank material that could be hauled per load were 14 percent for sand—gravel alluvia excavated without ripping, 28 percent for weathered rock—earth mixtures excavated by ripping, 49 percent for well-blasted rock with good fragmentation, and 67 percent for poorly blasted rock (based on observations in limestone and shale). These values reflect transfer of material from a stockpile using a front-end loader into a hauler.

DRAFT

DRAFT

For conditions where loose excavated material is compacted in a fill or embankment, the swell factor is reduced relative to that for the loose condition. Where the compacted swell factor is negative, it is referred to as a shrink factor. Percentage swell from the natural bed to the compacted condition is calculated as

$$Swell_c (\%) = 100 \cdot \left(\frac{\gamma_{in-situ}}{\gamma_{compacted}} - 1 \right) \quad 2-2$$

where $\gamma_{compacted}$ is weight in the compacted condition or compacted bulk density. Percentage swell from *in-situ* to compacted condition is equivalent to bulking factor after application of mechanical compaction with rollers, often with wetting of the fill. Church (1981) notes that certain friable rocks in weathered or parent rock zones have low swell factors from cut to fill and are equivalent to rock–earth mixtures in their behavior during excavation and compaction. In addition, rock swell factors are related to solid rock in the cut and do not include allowances for overlain residual and weathered rocks or for earth and friable materials, all of which would tend to reduce the swell factor from cut to fill.

Church (1981) provides representative values of swell factors for material excavated by various methods for use as fill. Residuals consisting of clays, silts, sands, and gravels tend to reduce in volume from cut to compacted fill by an average of 12 percent. Rippable rock (generally weathered rock consisting of a mixture of rock particles and some earth) tends to increase in volume by about 8 percent from cut to compacted fill. Blasted rock in the first stage of blasting contains 25 to 30 percent voids depending on the amount of fines created during blasting, corresponding to swell factors of 33 to 50 percent. Even in the absence of subsequent compaction, these high swell factors often are reduced in fill material due to the loading effects of haulers, tractor-bulldozers, water wagons, and other heavy moving machinery. For construction purposes, blasted rock is usually mixed with residuals and rippable rock to increase compaction, thus reducing the swell factor to a range of 8 to 18 percent after compaction.

Duncan, et al. (1972), cited by John Gale in CRWMS M&O (1998), documents a study of seepage and groundwater effects associated with explosive cratering for the Pre-Schooner and Danny Boy projects in the Buckboard Mesa basalt of the Nevada Test Site. As part of this study, the characteristics of granular ejecta (i.e., material thrown out above and beyond the crater) and material in the fallback zone of the craters were investigated. Trenches were dug through the ejecta material to determine its properties. The ejecta and fallback materials were considered to have similar physical properties based on prior investigations. While the study focused on evaluating permeability characteristics of the various zones around and within each crater, the findings are relevant in terms of identifying factors that influence bulking factor and means of estimating bulking factor.

According to Duncan, et al. (1972), the increase in porosity ($\Delta\eta$) of the postshot material relative to its preshot condition is related to bulking factor (B) by the following expression

$$\Delta\eta = 1 - \frac{1}{1+B} \quad 2-3$$

DRAFT

DRAFT

Bulking factor in this case is related to the ratio of pre-shot (*in-situ*) and postshot (loose) bulk density as follows

$$B = \frac{\gamma_{in-situ}}{\gamma_{loose}} - 1 \quad 2-4$$

Bulking factors of between 39 and 70 percent were measured for the ejecta from the various trenches excavated. Duncan, et al. (1972) noted that some sorting of the material, including removal of some fines, may have occurred during the blasting process, particularly in the ejecta.

Duncan, et al. (1972) measured particle size distributions of the excavated material using sieve analysis for particles less than 0.3 m [1 ft] in their intermediate dimension and direct measurement for larger particles. Comparative particle size distributions were developed using two photographic techniques: the photogrid area method and the photogrid point count method. Both methods use vertical photographs composed of approximately 3 by 3-m [10 by 10-ft]-square areas subdivided into 0.3-m [1-ft]-square areas. For the area method, the percentage of the surface covered by particles of a given size group was determined. In the point method, the size of the particle beneath each grid intersection point was estimated. Both of the photographic methods tend to produce coarser distributions than conventional mechanical analysis because they are relatively insensitive to smaller particle sizes. Particles coarser than 19 mm [3/4 in] were predominately angular in shape and were not flat or elongated. Below 19 mm [3/4 in], particles were found to be increasingly flat and elongated.

Using the properties determined for the ejecta, Duncan, et al. (1972) evaluated a number of permeability equations. The Kozeny-Carmen equation was selected to assess the influence of porosity, tortuosity, particle shape, and pore shape on the permeability of granular porous media. The estimated permeability was most influenced by the amount and distribution of the finest grained particles. For permeability estimates, the analysis of particle size distributions was recommended to extend down to the size for which only 1 percent of the particles was smaller. Although not identified specifically in this study, the porosity, and by inference, the bulking factors of the samples, were also potentially affected by the particle size distribution and particle shape.

Sandia National Laboratories (2007) recommended a bulking factor range of 10–40 percent for the analysis of rubble quantities for seismic consequences abstraction. Their recommendation was based on a review of bulking factor information from several sources, such as Laubscher (1994), Duncan, et al. (1980), and Bechtel SAIC Company, LLC (2004). In a state-of-the-art paper on cave mining, Laubscher (1994) suggested caved rock bulking factor values of 16 percent for fine fragmentation, 12 percent for medium fragmentation, and 8 percent for coarse fragmentation. Duncan, et al. (1980) reported graded rock fill for dams with bulking factors between 30 and 56 percent based on measured porosity values of 23 to 36 percent. Bechtel SAIC Company, LLC (2004) used the numerical code UDEC to estimate bulking factors for lithophysal zones in welded tuff based on modeling the rock mass as an assemblage of equant blocks with a characteristic length of 0.2 m [0.66 ft]. The model produced bulking factors of 19–25 percent.

DRAFT

2.2 Bulking Factor in Surface Excavation

For earthworks, estimates of bulking factor are typically based on in-place and excavated volumes. Volumes are estimated using one or more of four methods (Church, 1981):

- The subdivision method, where a large volume is broken into smaller volumes of known geometric shape and volume, then added together to estimate the total volume. Estimated precision for this method is ± 0.5 percent.
- The prismatic formula method, where the excavated or in-place volume resembles a prismoid, and volume is calculated using a closed-form solution. The estimated precision of this method depends on how closely the excavated volume resembles a prismoid.
- The average-end-area method, which is based on cross sections taken at regular intervals to estimate volumes between sections. Estimated precision of this method is about ± 1.0 percent.
- The contour method directly compares excavated contours with original contours to estimate the excavated volume. Estimated precision of this method is similar to that for the average-end-area method.

Placer mining and excavation of aggregate typically deal with granular soils. Peele (1961) suggested the average bulking factor for granular soil when first loosened depends on the grain size distribution and indicated typical values for soils: 14 percent for clean sand and gravel; 20 percent for loam and loamy sand or gravel; 35 percent for dense clay and dense mixtures of gravel and clay; and 50 percent for unusually dense gravel and clay as from a river bed. The bulking factor for gravel can range from 20 to 30 percent depending on the degree of fines mixed in with the gravel and may be up to 50 percent for compact clayey gravel.

Goktepe and Lav (2004) examined bulking of excavated materials because cut-fill balancing and minimizing the amount of earthwork are significant factors that can decrease highway construction costs. The authors presented a method to balance the cut-fill volume and minimize the amount of earthwork by accounting for shrink and swell factors, among other considerations. The swell factor has the same definition as bulking factor in this approach. Although it can range from zero to 100 percent, the swell factor typically does not exceed 40 percent for most surficial materials. Detailed investigation and determination of swell factor was beyond the scope of this report. Goktepe and Lav (2004) cited several highway engineering publications with respect to determining swell factor for excavation projects.

Wilkinson (1997) compiled information on typical bulking factors for excavated materials along with other pertinent properties. His results are summarized in Table 2-1. The shrinkage factor in Table 2-1 is the volume after compaction with mechanical equipment relative to the volume before excavation. The values of bulking factor for rock and some soil materials in Table 2-1 are identical to those Church (1981) published.

DRAFT

Table 2-1. Typical Bulking Factor Values for Surface Excavation

Material	Bulk Density Mg/m ³	Bulking Factor (Percentage)	Shrinkage Factor
Clay (Low Plasticity Index)	1.65	30	—
Clay (High Plasticity Index)	2.10	40	0.90
Clay and Gravel	1.80	35	—
Sand	2.00	5	0.89
Sand & Gravel	1.95	15	—
Gravel	2.10	5	0.97
Chalk	1.85	50	0.97
Shales	2.35	50	1.33
Limestone	2.60	63	1.36
Sandstone (Porous)	2.50	60	—
Sandstone (cemented)	2.65	61	1.34
Basalt	2.95	64	1.36
Granite	2.41	72	1.33

2.3 Bulking Factor in Underground Mining

2.3.1 Hard Rock Mining

With respect to underground mining of rock, Peele (1961) estimates in-place versus broken rock bulk densities, from which bulking factor can be deduced according to Eq. 2-1. Calculated bulking factors are shown in Table 2-2 for some common rock types. The values in this table are greater than the values from Church (1981), but fall within the uncertainty Church (1981) specified (Table A-1).

The slightly higher values may be because some fines generated in the mining process may be lost in the extraction and haulage of mined material. For hard rock broken by a crusher, the bulking factor is on the order of 35 percent if all sizes are mixed and the stone is shaken slightly. Conversely, for screened material where some fines are eliminated from the grain size distribution, the bulking factor for each screened portion typically ranges from 45 to 48 percent. Hard rock blasted in large pieces and loaded into cars typically has a bulking factor between 66 and 84 percent as shown in Table 2-2.

Three examples of rock embankments in Colorado, Virginia, and Ohio that Peele (1961) provided had bulking factors of 51 percent based on 2,752 m³ [3,600 yd³] of solid rock, 80 percent based on 38,228 m³ [50,000 yd³] of limestone and mica schist, and 65 percent based on 79,160 m³ [103,537 yd³] of subaqueous excavation. These values represent clean broken rock without fines and are similar to those in Table 2-2. The platy nature of mica schist at the Virginia site accounts for the increased bulking factor for the embankment compared to the other sites. These results indicate that the gradation of the material and rock type affect bulking factor. Materials with fine particles removed tend to exhibit larger bulking factors compared to similar materials with fine particles retained.

DRAFT

Table 2-2. Typical Bulking Factors for Mined Rock			
Rock Type	Bulk Density (tons/yd³)		Bulking Factor (Percentage)
	In-place	Broken	
Dolomite	2.16	1.30	66
Gneiss	2.27	1.30	75
Granite & Porphyry	2.30	1.31	76
Greenstone & trap	2.52	1.39	81
Limestone	2.27	1.30	75
Quartz	2.23	1.27	76
Sandstone	2.08	1.16	79
Slate	2.36	1.28	84

Richards, et al. (2002) performed a geotechnical investigation of the formation of ground collapse craters over abandoned mine workings in Waihi, New Zealand. Underground mining of gold-silver-bearing quartz lodes or reefs was carried out at Martha Hill from 1882 until 1952, with shafts and workings reaching a total depth of approximately 600 m [1,968 ft] on 16 levels to mine the steeply dipping ore bodies. Subsequent open pit mining operations were initiated in the same area to extract remaining identified ore reserves. The investigation included a review of bulking factor information, with the following findings.

- (1) When *in-situ* soils and rocks are excavated volume increases from 15 to 80 percent depending on the type of material, the excavation method, and the range of particle sizes it is broken into. Typically, strong rocks break into more uniform blocky pieces than do weak rocks and soils, and broken material derived from strong rocks therefore has a larger proportion of voids space and hence a higher bulking factor.
- (2) Bulking factors for rock are typically in the range of 33–50 percent. Gilmour and Johnston (1912) note that 40 percent of the Waihi ore had to be drawn off the shrinkage stope after each blasting round to maintain working space for the next round, indicating a bulking factor of 40 percent for the quartz ore. Church (1981) gives bulking factors of 50 percent and greater for rocks similar to andesite. Blyth and De Freitas (1990) give bulking factors of 50–80 percent for unweathered, blocky igneous and metamorphic rocks, and 25–40 percent for weathered igneous and metamorphic rocks. Bell and Stacey (1992) give a typical range of bulking factors of 30–50 percent for coal measures strata. Whittaker and Reddish (1989) give bulking factors ranging from 33–50 percent.
- (3) Based on these data, Gilmour and Johnston (1912) selected a bulking factor of 41 percent as a representative middle range value for the collapsing stopes at Waihi, where the collapsed rock mass is likely to be in a loose arrangement with relatively high void space.
- (4) Experience with stockpiles at Waihi indicates bulking factors of 15–30 percent (mean 23 percent) for material excavated from the open pit. Stockpile bulking factors might represent materials that had been broken down into a wider range of particle sizes and hence have fewer voids and a smaller bulking factor because of being broken by blasting and worked with machinery.

Richards, et al. (2002) concluded that a reasonable range for bulking factor of rockfall rubble in hard rock was 15–50 percent for the purposes of a risk assessment of further collapse potential.

DRAFT

2.3.2 Caving Methods of Mining

Caving methods of underground mining use controlled collapse of the orebody into the underlying mined opening and withdrawal of the collapsed material at a rate to maintain controlled extraction of the ore. In block caving, ore masses, ore panels, or ore blocks are undercut to induce controlled caving of the orebody, with the broken rock drawn off from below. According to Brady and Brown (2004), there is a relation between the natural rate of caving and the permissible rate of draw of the caved material. During the process of caving, the ore will increase in volume, or bulk, with a bulking factor on the order of 20 percent for initial caving. For caving to proceed successfully, the volume drawn after each episode of caving should be only the difference between the *in-situ* and bulked volumes of the newly caved ore, sometimes referred to as the swell.

The block caving process is influenced by the nature of the caved material, particularly the block size and characteristics. The shape and size of rock blocks are controlled largely by existing discontinuities. Brzovica and Villaescusa (2007) described fragmentation size predictions at the El Teniente copper mine in Chile, employing stochastic simulations of rock structure based on structural data collected using mainly line mapping techniques in mine drives. The main rock types at this site include andesite, diorite, and hydrothermal breccias. The authors undertook a detailed characterization of rock blocks. The caved rock block description included geometrical and face characteristics similar to those established during line mapping. Particular data collected included volume, shape, number of faces, edge length, and dihedral angle between a pair of faces. The investigation found that filled veins within the rock mass contributed to block fragmentation during caving. Truncation biases applied during data collection strongly affected the calculated discontinuity set parameters such as spacing and distribution of thicknesses, and the *in-situ* block size distribution. These factors are important in estimating block size distributions.

Dunrud (1998) investigated relationships among bulking factor and the shape and height of caving above an underground mine opening. For a mine opening of height h and rock with a bulking factor of 25 percent, the caved zone height can reach $4h$ for a rectangular prism, $6h$ for an ellipsoid, $8h$ for a wedge, and $12h$ for a cone. Dunrud (1998) noted the actual bulking factor varies from least to greatest from the base of caved rubble upwards because of compaction induced by self-loading. Examples of rubble in caved openings illustrated that small caved fragments of shale exhibited a lower bulking factor than large blocks of jointed sandstone and siltstone.

In describing the process of block caving of weak rock masses associated with metal mines, Bétournay (2004) assumed an ellipsoidal caved zone. The dimensions of the caving volume were obtained by calculating the amount of caved material that would fill the underlying void using a bulking factor between 10 and 40 percent, representative of fine rock mass fragments to blocky ground. In a prior publication on the surface effects of underground mining, Bétournay (2002) indicates that chimneying disintegration in hard rock mines occurs in weak rock units such as schist or altered rock with a bulking factor between 5 and 20 percent.

A case history of the Questa molybdenum mine near Taos, New Mexico (Gilbride, et al., 2005), determined the bulking factor for two distinct mining blocks based on volumetric considerations. The lithology at the mine comprises andesite, felsic and intermediate dikes, and aplite-porphyry rocks. The rock mass rating based on the tunnelling quality index Q varies from exceptionally poor to fair. Block caving of the Goathill Orebody to date has produced a large mature draw cone. The volumetric difference between the total underground extraction {8.2 million m^3

DRAFT

DRAFT

[290 million ft³] and volume of the glory hole {4.7 million m³ [166 million ft³]} indicates a gross cave bulking factor of 9–21 percent assuming that the zone of bulking is defined by cave angles of 70–85°. The D Orebody Block 1 is a relatively recent development with 50 percent of the ore column extracted by 2004. Based on the breakthrough of the cave to surface, a bulking factor of no greater than 10 percent was estimated for the orebody. A numerical modeling of the caving using the discrete element code PFC3D indicated a similar value gross bulking factor.

2.3.3 Underground Coal Mining

In longwall coal mining, the caved rock behind the advancing longwall face is known as the gob. The gob is formed by rock fragments that fall from the roof strata into the cavity created by the removal of the coal bed and can exhibit large void ratios (i.e., large bulking factor).

The bulking-factor-controlled caving model is widely used to calculate the height of the caved zone (Palchik, 2002). The model gives the caved zone height (H) in bedded rocks as a ratio of the working height of underground coal extraction (h) to the bulking factor (B)

$$H = \frac{h}{B} \quad 2-5$$

(i.e., where bulking factor is the increase in volume of rock due to caving relative to its initial volume). Trueman (1990) suggested in a finite element analysis of stresses associated with coal mine caved waste that a bulking factor of 50 percent is representative of the majority of U.K. coal mining conditions.

Unrug (1982) demonstrated that the height of the caved zone partially depends on the character of the immediate roof strata, with bulking factors generally in the range of 20–50 percent. Thicker strata with relatively low fracture frequency may not collapse completely due to interlocking of blocks and may form a stable arch. In a review of the relation between bulking factor of the immediate roof rock in coal mining and required shield capacity for ground support, Barczak (2006) found that the shape of rock fragments (or blocks) affects bulking factor. More competent strata found in some U.S. mines caved in more blocky fashion with less of a bulking factor than weaker, more friable roof geologies found in most European mines.

In determining the immediate roof at mines of the Kutahya-Omerler coal basin in Turkey, Konak, et al. (2006) analyzed measured convergence and load cell data to back analyze bulking factor. In this case, the volumetric comparison method was used in a gallery with an 8-m² [86 ft²] cross section to estimate the increase in volume of blasted rock, resulting in an estimated bulking factor of 47 percent. Das (2000) found that the ultimate *in-situ* bulking factor of coal measure strata at a longwall face in a coal mine in India was less than 5 percent and decreased exponentially with increasing caving height. In this case, caving was controlled by the thick blocky nature of the overlying strata, resulting in a relatively orderly arrangement of caved gob material. These examples illustrate the important influence of stratigraphy and structural geology on bulking factor.

Esterhuizen and Karacan (2007) indicated the bulking of the gob is affected by the fall height, as well as the size and shape of the rock fragments. When the fall height is larger than the lateral dimension of the rock fragments, the fragments are more likely to rotate and come to rest in an open disorderly arrangement with large void ratio. This is known as fully caved rock (Figure 2-3A). As caving proceeds upwards, the caved rock occupies a progressively

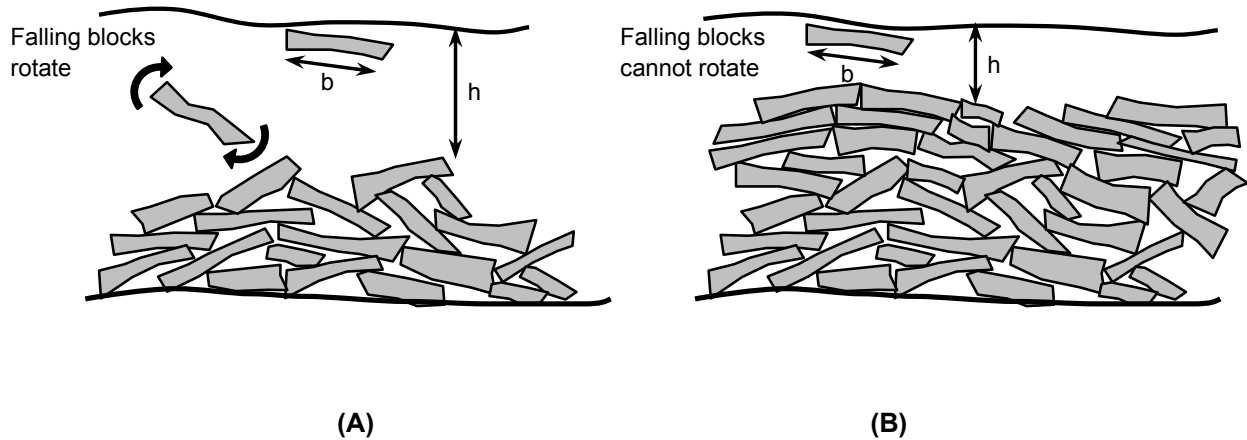


Figure 2-3. Schematic Illustrating the Effect of Fall Height on Void Space Between Gob Fragments. Voids Reduce as the Ratio of Fall Height (H) to Block Width (B) Decreases Because Rotation of Individual Fragments Is Inhibited (After Esterhuizen and Karacan, 2007).

increasing proportion of the free space, thus reducing the fall height of the subsequent fragments. As the fall height decreases, the potential for fragments to rotate diminishes and the amount of bulking is reduced. This is known as partially caved rock (Figure 2-3B). As mining progresses, the gob is gradually compacted by the weight of the overburden, resulting in a reduction in the void ratio. These effects suggest that bulking factor is not constant within a caved rubble pile and may change with time as the overlying overburden deforms and applies pressure to the accumulated rubble.

Esterhuizen and Karacan (2007) estimated the variation in bulking of the gob in the vertical direction using a procedure Munson and Benzley (1980) suggested. The procedure assumes that maximum bulking of the caved rock will occur when the fall height exceeds about twice the block width. The maximum bulking factor was assumed to be 75 percent based on tests of simulated gob materials (Pappas and Mark, 1993). Figure 2-4 shows the relation between the ratio of fall height to block width (h/b) and bulking factor for the gob in a longwall coal mine. This relation suggests that bulking factor may decrease with increasing block size in an opening of a given height. Alternatively, larger openings in a particular rock mass comprising a given block size may result in larger bulking factors in accumulated rubble than smaller openings of the same shape and orientation. Bulking factor of rock has been shown to increase with increasing rock strength (Palchik, 2002). Based on studies of small coal mines operated in the Donetsk area of Ukraine, with strong rock at intermediate and greater depths of longwall mining, the bulking factor was found to depend on the square root of uniaxial compressive strength of the immediate roof

$$B = a\sqrt{\sigma_c} \quad 2-6$$

where σ_c is the uniaxial compressive strength of the immediate roof in MPa and a is an empirical coefficient [$a = 0.05$ for carbonate rocks in Donetsk area (Palchik, 2002)]. For uniaxial

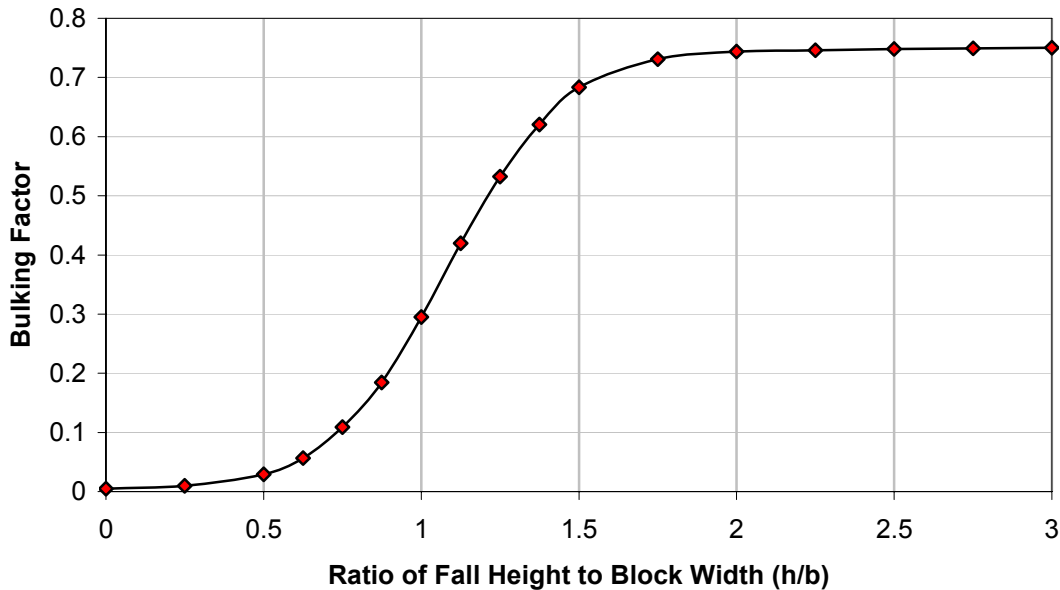


Figure 2-4. Relation Between Ratio of Fall Height to Block Width (H/B) and Bulking Factor for Longwall Coal Gob (After Esterhuizen and Karacan, 2007)

compressive strength of 25–150 MPa, using $a = 0.05$ in Eq. (2-6) results in bulking factors of 25–61 percent.

For weak rocks (argillite, sandy shale, and sandstone) with compressive strengths less than 11 MPa and porosity of 23–47 percent, Palchik (2002) determined that the ratio of caved zone height to mine opening height H/h was inversely related to the root of the fourth power of the uniaxial compressive strength of the immediate roof rock. Palchik (2002) also found that the ratio H/h was directly proportional to the average porosity of rock layers overlying the immediate roof. From Eq. (2-5), the ratio H/h is the reciprocal of bulking factor. Palchik (2002) used these relationships to calculate bulking factors of 8–24 percent for the weak rock of the Donetsk area. Compared to the values for strong rock in the same area, bulking of the immediate roof in weak rock is less significant in limiting the formation of the caved zone over the underground opening than in strong rocks. Palchik (2002) determined the height of the caved zone above the original mined opening by drilling. The underground openings in the old mines were mainly drifts along short {(25–28 m [82–92 ft])} coal faces. Physical properties of the rock were determined through laboratory testing.

DRAFT

Pappas and Mark (1993) studied properties of longwall gob materials to determine stiffness values for use in numerical modeling. Noting a large uncertainty in published estimates of tangent and secant moduli of gob material, Pappas and Mark (1993) performed a series of laboratory tests on simulated gob material from three mines. The simulated material comprised broken rock obtained from fresh rockfalls and was selected to have the same characteristics of actual gob material, including tensile and compressive strength, density, surface roughness, particle shape, particle size, and size gradation. To conduct laboratory-scale testing, the maximum rock size was reduced, and the gradation curve was shifted parallel to itself to the desired maximum particle size for the laboratory tests. This approach was based on prior work by Marachi, et al. (1969), Fumagalli (1969), and Becker, et al. (1972), who demonstrated that particle size distribution curves for actual dam rockfill materials could be proportionally scaled down to obtain representative laboratory-scale specimens for testing.

Pappas and Mark (1993) determined the gradation curve for gob material using photoanalysis techniques applied to photographs of *in-situ* gob material. Franklin, et al. (1988) described a similar technique using photoanalysis software. The technique involves tracing the outline of photographed gob material, using a scale in the photograph to estimate size and frequency of rock fragments so that a histogram can be compiled. Data are then plotted as “rock size” versus “mass percentage smaller than each size” to generate a gradation curve for the gob rock. The gradation curves are then adjusted to account for rock fragments hidden by the two-dimensional nature of the photograph, and for smaller particle sizes not observable in the photograph, by comparing a photo-derived gradation curve of piled rock rubble with a mechanically measured gradation curve for the same material. The photoanalysis technique accurately estimated the actual gradation curve of the rock material with the exception of the smaller particle sizes, which the technique underestimates.

Pappas and Mark (1993) tested three rock types (shale, strong sandstone, and weak sandstone) using simulated gob samples with the maximum particle size set to approximately 90 mm [3.5 in] to satisfy requirements of the testing apparatus. The laboratory tests were performed to assess how maximum particle size, particle shape, particle breakage, void ratio, and rock strength affect the stress–strain behavior (i.e., the tangent and secant moduli) of the simulated gob material. Bulking factor was considered as part of this assessment. The source materials were characterized for appearance using a method Ferm and Smith (1980) described, for overall shape of the rock (disk, blade, spheroid, or roller) using Zingg’s method as Pappas and Mark (1993) described, and for density and strength using standard ASTM methods. The number of contact points per particle was determined by saturating the simulated gob sample with white paint, then counting the number of unpainted contact points on a number of representative rock fragments.

Testing apparatus comprising a 36.3-cm [14.3-in]-diameter test chamber and a loading platen was developed to assess the load-deformation response of the granular materials. As part of the test procedure, rock from each size class of the gradation curve was weighed out and evaluated for shape effect by measuring the length, width, and thickness of representative fragments. The weight of rock in the chamber was measured to determine void ratio at the start of the test. A servo-controlled loading frame was used to apply load at a preset ramp rate, and displacement of the platen was measured using linear variable differential transducer. Following the test, the rock material was resieved to assess particle breakage, and sample fragments were measured to determine changes in particle shape.

The test results produced nonlinear stress–strain curves for each of the samples tested, indicating increasing stiffness with increasing load. Void ratio (defined as the ratio of void

DRAFT

DRAFT

volume to the *in-situ* volume of rock; equivalent to bulking factor) was calculated throughout each test. Initial void ratios for the three rock types were about 0.77 for weak sandstone, 0.82 for shale, and 0.86 for strong sandstone. With increasing load, the void ratio decreased in each case. For weak sandstone and shale, the tangent modulus remained relatively constant until the void ratio decreased to about 0.40, at which point the tangent modulus started to increase exponentially with increasing load. For strong sandstone, the same trend was evident, but the transition to exponentially increasing tangent modulus occurred at a void ratio of about 0.55. The transition from constant to exponentially increasing modulus was attributed to rock breakage, producing fines to fill voids, and thereby increasing the rock stiffness. Bulking factor values measured at a load of 800 psi ranged from 27–31 percent for shale (with a value of 14 percent for a uniformly graded sample), 31–34 percent for weak sandstone, and 47–50 percent for strong sandstone.

Statistical analysis of the test results (Pappas and Mark, 1993) suggested that void ratio, secant modulus, tangent modulus, and most of the shape ratios were significantly affected by rock type, whereas changes in the maximum particle size did not affect any of the variables. Gradation curve shape also affected the compressibility of the simulated gob material. Multiple regression analysis was used to develop relations between the various parameters. Bulking factor, tangent modulus, and secant modulus, were each found to be a function of rock strength and thickness-to-width shape ratio. Pappas and Mark (1993) describe the bulking factor relationships using the following equation

$$B = ax_1 + bx_2 + c \quad 2-7$$

where x_1 is rock strength (in MPa); x_2 is the thickness-to-width shape ratio (dimensionless); and a , b , and c are derived parameters that are dependent on stress level. Values for these parameters are shown in Table 2-3. The values for a in Table 2-3 were converted from the values Pappas and Mark (1993) provided to be consistent with rock strength expressed in MPa. Likewise, the values for c were converted to express bulking factor in terms of B as defined in Eq. (1-1) (i.e., change in volume of rubble relative to the original *in-situ* volume of rock). Pappas and Mark (1993) had expressed bulking factor in terms of B_1 as in Eq. (1-2) (i.e., ratio of rubble volume to the *in-situ* rock volume).

Table 2-3. Derived Parameters Relating Bulking Factor to Rock Strength and Shape Ratio*				
Overburden Stress		Multiple Regression Analysis Factors		
(psi)	(MPa)	<i>a</i>	<i>b</i>	<i>c</i>
400	2.758	2.669×10^{-3}	0.267	0.160
600	4.137	2.944×10^{-3}	0.274	0.060
800	5.516	2.712×10^{-3}	0.262	0.040
1,000	6.895	2.683×10^{-3}	0.269	-0.008
1,500	10.342	2.321×10^{-3}	0.209	0.000
2,000	13.790	2.176×10^{-3}	0.221	-0.037
2,500	17.237	1.973×10^{-3}	0.247	-0.069

*Pappas, D.M. and C. Mark. "Behavior of Simulated Gob Material." Washington, DC: Report Investigations RI 9458. U.S. Department of Interiors. 1993.
 Note: Factors adjusted for rock strength to be expressed in MPa
 $B = ax_1 + bx_2 + c$

DRAFT

DRAFT

A curve-fitting analysis using linear regression for parameters a and b and a power law for parameter c was performed to develop a general relation for bulking factor as a function of overburden stress (stress imposed by the weight of any overlying material), rock strength, and thickness-to-width ratio. The analysis resulted in the following expression for bulking factor

$$B = (a_1\sigma_v + b_1)x_1 + (a_2\sigma_v + b_2)x_2 + (a_3\sigma_v^{b_3} + c_3) \quad 2-8$$

where σ_v is the overburden stress (MPa), x_1 is rock strength (MPa), x_2 is the thickness-to-width ratio (dimensionless), and the curve-fit coefficients are as follows:

$$\begin{aligned} a_1 &= -6.132 \cdot 10^{-5} & a_2 &= -3.062 \cdot 10^{-3} & a_3 &= 0.691 \\ b_1 &= 3.028 \cdot 10^{-3} & b_2 &= 2.764 \cdot 10^{-1} & b_3 &= -1.023 \\ c_3 &= -0.089 \end{aligned}$$

Applying Eq. (2-8) to the range of shape ratios and rock strength values Pappas and Mark (1993) provided resulted in the family of curves shown in Figure 2-5. Although the curves are based on laboratory tests for three specific rock types with known gradation, the results indicate a nonlinear relation between bulking factor and overburden stress. The information in Figure 2-5 indicates that bulking factor is strongly affected by rock strength and, to a lesser extent, rock fragment shape. For rocks with relatively low bulking factors under gravity loading in piles of loose material, bulking factor may be significantly reduced as the height of overlying material increases.

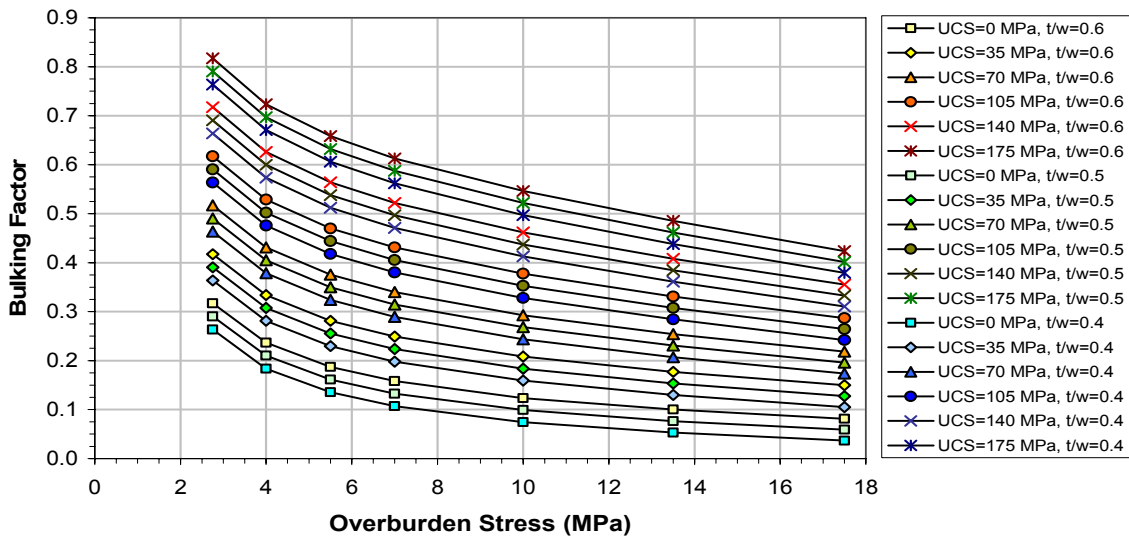


Figure 2-5. Relation Between Overburden Stress and Bulking Factor for a Range of Unconfined Compressive Strength (UCS) and Thickness-To-Width Ratios (T/W). Results Are Based on Laboratory Testing of Simulated Gob Material From Three Longwall Coal Mines, Including Shale, Weak Sandstone, and Strong Sandstone (After Pappas and Mark, 1993).

DRAFT

As Pappas and Mark (1993) pointed out, bulking factor of the actual gob material is likely dependent on its position within the accumulated rubble and the point in time that it is evaluated during the longwall process. Immediately after the roof fall that creates the gob, the bulking factor will start to decrease as the gob gradually takes on more load and further compacts. Also, other unknown factors and potential first-order effects such as bulking factor gradation, caving height, and degree of fracturing of the immediate roof make it difficult to predict material properties at a specific location within the gob. Comparing laboratory test results with closed-form solutions for tangent modulus and secant modulus demonstrated that the published solutions could be calibrated on the basis of laboratory testing data to predict modulus values for numerical modelling of gob behavior. The gradations used in the simulated gob material in the Pappas and Mark (1993) study were based on photographs from mines in the central Appalachian region, which characteristically consist of competent rock. Changing the gradation of the simulated gob material is expected to affect the bulking factor. Pappas and Mark (1993) cited a laboratory test that indicates a gob material composed of a greater proportion of uniformly sized rock fragments will have more void spaces and greater bulking factor.

Yavuz (2004) described an empirical criterion predicting the extent of the caving zone developed in China from a diverse data set for mining environments with different lithological and geometrical characteristics. For flat or nearly flat coal seams where longwall mining has been employed, the bulking factor is given by the following relation.

$$B = c_1 h + c_2 \quad 2-8$$

where B is bulking factor (%), h is height of the mined opening (m), and c_1 and c_2 are coefficients related to rock strength as shown in Table 2-4. The predicted bulking factors for openings of various heights in Table 2-4 indicate an inverse relationship between rock strength and bulking factor, contrary to the findings of Palchik (2002) and Pappas and Mark (1993). This discrepancy exists because the caved rubble tends to have an orderly arrangement in these cases; therefore, less broken rubble has a lower bulking factor.

Salamon (1990) described mechanisms of caving in longwall coal mining. Bulking factor depended on applied vertical pressure according to the following relation.

$$B = [(p + (B_0 + 1)p_c)/(p + p_c)] - 1 \quad 2-9$$

where p is pressure, B_0 is initial bulking factor, and p_c is a material constant. Eq. (2-9) indicates bulking factor decreases as pressure increases.

Strata Lithology	Compressive Strength (MPa)	Coefficients		Predicted Bulking Factor		
		c_1	c_2	$h = 2.5 \text{ m}$	$h = 4.0 \text{ m}$	$h = 5.5 \text{ m}$
Strong and hard	>40	2.1	16	21.3	24.4	27.6
Medium strong	20-40	4.7	19	30.8	37.8	44.9
Soft and weak	<20	6.2	32	47.5	56.8	66.1

*Yavuz, H. "An Estimation Method For Cover Pressure Re-Establishment Distance and Pressure Distribution in the Goaf of Longwall Coal Mines." *International of Journal Rock Mechanics and Mining Sciences*. Vol. 41. pp. 193-205. 2004.

DRAFT

Sweby (1997) reviewed caving mechanisms around high extraction systems in South African coal mines to determine the effect of the mechanisms on safety. Caving in this context refers to the process of fracture and collapse of the overlying strata in response to total extraction of a coal seam. The key results follow.

- (1) Borehole extensometer observations at the Sigma Colliery were taken of a 40-m [131-ft]-thick shale–sandstone parting above the mined coal seam and below an overlying massive dolerite sill to determine the caving height. Bulking factors estimated from 4 boreholes were 15, 20, 30, and 40 percent, suggesting that bulking factor can vary considerably depending on immediate roof conditions.
- (2) In the Highveld Coalfield, caving of sandstone/siltstone strata overlying a coal seam was monitored using borehole extensometers. The calculated bulking factor of the immediate roof was 13 percent, with the height of caving reaching 17 m [56 ft] above the seam.
- (3) Experimental work conducted at the Twistdraai Colliery, Sasol Coal determined that caving at this site usually occurs in a series of falls. Rockfalls occurred suddenly and in clearly defined successive steps, each associated with a homogeneous lithologic unit and occurring in large blocks. The rock units overlying the coal seam were sandstone and siltstone. The maximum caving height was 75 m [246 ft], with a corresponding bulking factor of 5 percent.

Sweby (1997) compiled average bulking factors for typical strata types occurring in the South African coalfields based on the work of several other researchers. These values (Table 2-5) were derived from measurements between discrete anchors situated in the active caving zone. As shown in Table 2-5, bulking factors for coarse to fine sandstone are higher than those for shale/siltstone. This may be related to both strength of the strata and the laminated nature of the more argillaceous strata. Greater caving height (i.e., lower bulking factors) would be expected in laminated strata.

Peng and Chiang (1984) discuss bulking factor in longwall mines, noting that bulking factor varies with rock type, shape and size of cave fragments, arrangement of caved fragments in the rubble pile, and the pressure imposed on the rubble pile. As Esterhuizen and Karacan (2007) discussed, caving height relative to fragment size affects the arrangement of fragments in the rubble pile; larger caving heights produce more disorderly arrangements of fragments and larger bulking factors. For orderly arrangements of fragments, stronger and harder rock will tend to form larger fragments and will exhibit lower bulking factors than weaker and softer rocks. For disorderly arrangements of fragments, the converse is true; the bulking factor of stronger and harder rocks will be larger due to relatively large rock fragments compared to weaker and softer rock with smaller fragments. Peng and Chiang (1984) provide bulking factor values for various rock types (Table 2-6), distinguishing between original bulking factor (i.e., the bulking factor of fresh rockfall rubble without an applied load from the overlying strata) and the residual bulking factor (i.e., the bulking factor once the full weight of the collapsed longwall roof is applied to the rubble pile).

DRAFT

	Lithology							
	Coal	Silt mudstone	Carbonaceous shale	Shale	Sandy shale	Shaley sandstone	Coarse sandstone	Fine sandstone
Bulking Factor	30%	10%	15%	20%	25%	30%	40%	50%

*Sweby, G. "Review the Caving Mechanisms Around High Extraction Systems and Determine the Effect of the Mechanisms on the Safety of the System." CSIR Miningtek Project No. COL-327, October 1997. Submitted to Safety in Mines Research Advisory Committee (SIMRAC). 1997.

Rock Type	Bulking Factor	
	Original Bulking Factor	Residual Bulking Factor
Sand	6–15%	1–3%
Clay	<20%	3–7%
Broken coal	<30%	5%
Clay shale	40%	10%
Sandy shale	60–80%	25–35%
Sandstone	50–80%	30–35%

*Peng, S.S. and H.S. Chiang. *Longwall Mining*. New York City, New York: John Wiley & Sons. 1984.

Peng and Chiang (1984) also mentioned a comparison of measured volumes of underground roof fall cavities with volumes of rock rubble piled on the floor of mine entry drifts in the Pittsburgh seam. The bulking factor for the roof shale ranged from 25 to 30 percent, with an average of 28 percent.

2.4 Measurement of Bulking Factor

Bulking factor can be measured in a number of ways. For granular materials, bulking factor has been determined by comparing the amount of loose material needed to fill a wooden box of volume 0.028–0.057 m³ [1–2 ft³] against the original excavated volume (Peele, 1961). This procedure is repeated for multiple locations to account for local variability in the deposit. For larger volumes or particle sizes of material such as surface excavation stockpiles and embankments, the general procedure involves estimating the excavated volume using one of several geometric approaches (Church, 1981) and comparing it to the in-place volume. This can be done using standard surveying techniques. Digital imaging techniques also can be used to create digital elevation models of the ground before and after excavation to estimate the in-place volume, and of the stockpiled material to estimate loose volume.

Church (1981) describes using the sand-cone method to measure *in-situ* density of compacted material in embankments. The method involves placing a steel base plate with a central 102-mm [4-in]-diameter hole on the ground, then excavating material through the hole to a specified depth. The excavated material is weighed. The hole is then filled with sand using an inverted cone placed over the hole. Knowing the sand density and the weight of sand in the hole determines the excavated volume. The bulk density of the original material is then calculated as the weight of excavated material divided by the excavated volume.

For rock in underground openings, bulking factor can be estimated by comparing bulk density of the broken rock material to the *in-situ* bulk density. *In-situ* bulk density can be determined from

DRAFT

DRAFT

core samples or by density logging in boreholes (Telford, et al., 1976). For rock containing large voids such as lithophysae, large samples may be needed to include representative distributions of the void spaces in the measurement. Similar measures of mass and volume of broken material of the same rock type are required for comparison. These measurements can be obtained by estimating the volume of a rubble pile from a rockfall, then gathering and weighing the broken material, or filling a vessel of known volume with broken material and determining its mass. In using this approach, it is important to ensure the particle size content of the rubble pile is adequately represented in the samples used for measurement.

An alternate approach is to compare the rubble pile volume to the *in-situ* volume detached during a rockfall. To monitor changes in the geometry of an underground opening, precision laser scanners and photo scanners can be used to conduct successive surveys. Unlike conventional tunnel survey approaches that require reflective prisms, these systems use a dense grid of laser pulses or stereographic camera images to map the three-dimensional surface of the opening. The devices can create a detailed surface map of an opening very rapidly. Successive images can be compared to calculate geometrical changes, volume changes, and areas of instability. In the event of localized failure, the geometry of the failed zone and the resulting rubble within the opening can be calculated as long as the instrument can be set up in the opening.

Another approach is to develop correlations between gradation curves of rockfall rubble and void ratio for a specific site. Once a correlation is established, estimated gradation curves can be used to infer bulking factor. According to Wang, et al. (2003), there are three common methods of assessing rock fragment size:

- (1) The index evaluation method estimates the fragment size by using either the RQD index, the fracture spacing index, the block size index, or the volumetric joint count index. These indices mainly consider the influence of joint spacing on the size distribution of rock blocks and only give the average dimension of the rock blocks.
- (2) Image-based measurement methods are used in measuring the size distribution of broken rock fragments by processing the two-dimensional images taken on the surface of a rock pile. These methods involve assumptions about transforming the two-dimensional measurements on the surface of the rock pile to the three-dimensional distribution of the fragment volumes inside the rock pile and therefore require calibration.
- (3) The dissection model outlines a general approach for deriving the *in-situ* size distribution of rock fragments from the analysis of simulated discontinuity networks. The simulated rock mass is made up of intersecting discontinuities. The fragmentation characteristics are derived from fitted distributions of two-dimensional measurements of the various geometrical parameters. The influences of random discontinuities, persistence of discontinuities, *in-situ* stress, and shear strength of a rock mass on the characteristics of rock fragmentation are rarely considered.

Wang, et al. (2003) demonstrated a new three-dimensional model for estimating the characteristics of ore fragmentation in block caving, based on a Monte Carlo simulation technique, using data from a northern China underground copper mine. The results showed good correlation between calculated and field measured block size distributions, except for blocks larger than 1.2 m [3.9 ft].

DRAFT

DRAFT

Each of these methods can be used to estimate the expected gradation curve for a particular rock mass. A correlation between gradation and void ratio is needed, however, to estimate bulking factor using gradation curves.

For active caving operations, borehole extensometers and other instruments have been used to identify the height of caving. Bulking factor is then back analyzed using a closed form solution, such as Eq. (2-5).

DRAFT

3 SUMMARY OF BULKING FACTOR INFORMATION

A summary of bulking factor information from the reviewed literature and laboratory test results from Appendix C is provided in Table 3-1. In each case, the literature reference is given, along with the material type considered, the bulking factor value, the context for the measurement, and the method used to estimate bulking factor. The table also includes a judgment of the relevance of each dataset for analyzing potential degradation of emplacement drifts in welded tuff at Yucca Mountain: “0” for not relevant or “1” for relevant. The factors considered in the judgment include (i) rock type (i.e., data obtained from a rock with properties similar to welded tuff were assigned a relevance factor of one, and data obtained for other rock types were assigned a relevance factor of zero) and (ii) mode of rubble formation (i.e., data obtained from rubble resulting from a natural or induced collapse of an underground opening were assigned a relevance factor of one, and data for rubble that was excavated or processed in any way were assigned a relevance factor of zero). This categorization resulted in 16 data values considered relevant to emplacement drifts in welded tuff (i.e., the data values in Table 3-1 that were assigned equal-weighted relevance factors), which are referred to hereafter as the “subset of 16.” The subset of 16 was used in statistical analyses described in the next section. An analysis of the entire data set in Table 3-1, with equal-weighted values (i.e., no consideration of higher or lower relevance between the relevant data values), was also performed to compare the subset of 16 with the entire data set.

Bulking factor information was also collected through analysis of field data from Fran Ridge, near Yucca Mountain (Appendix B). The field data includes plots of rubble shape and size distributions that could be used to estimate bulking factors. Although literature information suggests general relationships among bulking factor, particle shapes and sizes, and other properties such as fall height and rock strength, the understanding of such relationships has not progressed enough to enable an estimation of bulking factor using particle size and shape distributions (such as provided in Appendix B). Therefore, the information in Appendix B has not been used to determine bulking factors and is not included in the data analysis discussed in this chapter.

To obtain an aggregate of bulking factor ranges from the literature review (Table 3-1), a simple, widely used approach for analyzing expert opinions (Ayyub, 2001) was applied to develop a composite probability distribution based on the surveyed literature. The approach is based on an equally weighted linear-averaging technique, which combines the individual expert information based on probabilistic considerations. Its implementation along with the assumptions made is described in the following.

Given the ranges provided and the equal weight assumption for each data input considered, a probability distribution $f_i(B)$ with mean μ_i and standard deviation σ_i was assumed for each set i (which varies from 1 to N , the number of expert inputs considered) with a constant weight w_i . For the current purposes, a uniform distribution with lower and upper limits a_i and b_i was chosen to reflect the lack of knowledge with regard to any tendencies in the individual input data. For

Table 3-1. Summary of Bulking Factor Information From Literature

	Reference	Material	Bulking Factor	Context	Method	Relevance Factor and Rationale	Comments
1	Bell and Stacey (1992)	Coal measure rocks	30–50%	Underground mining	Unknown	=0= Coal measure rocks may result in rubble properties different from welded tuff	Results quoted in Richards, et al. (2002).
2	Bétournay (2002)	Schist, altered rock	5–20%	Hard rock mining	Volume	=0= Altered schist may break in small platy particles, therefore resulting in rubble properties different from welded tuff	Rockfall due to chimneying disintegration
3	Bétournay (2004)	Weak rock masses	10-40%	Hard rock mining	Volume	=0= Geologic description suggests a rock type that may result in rubble properties different from welded tuff	Typical range for finely fragmented to blocky ground
4	Blyth and De Freitas (1990)	Unweathered blocky igneous and metamorphic rocks	50–80%	Underground mining	Unknown	=1= Geologic description suggests rock types generally similar to welded tuff	Results quoted in Richards, et al. (2002)
		Weathered blocky igneous and metamorphic rocks	25–40%	Underground mining	Unknown	=1= Geologic description suggests rock types generally similar to welded tuff	Results quoted in Richards, et al. (2002)
5	Brady and Brown (2004)	Hard rock ore	20%	Block caving mining	Volume	=0= Information provided is insufficient to permit determination of relevance	Bulking factor associated with initial caving
6	BSC (2004)	Lithophysal zones in welded tuff	10–40%	Emplacement drifts	UDEC modeling	=1= Information calculated for Yucca Mountain welded tuff	Based on model with 0.2-m [0.66-ft] characteristic length

Table 3-1. Summary of Bulking Factor Information From Literature (continued)

	Reference	Material	Bulking Factor	Context	Method	Relevance Factor and Rationale	Comments
7	Church (1981)	Tuff	50% (loose) 33% (compacted)	Excavation (general)	Literature	=0= Information provided is insufficient to permit determination of relevance	Average values with $\pm 33\%$ variance
		Default value assigned to any rock for which a value was not available	67%	Excavation (general)	Literature	=0= Information based on materials that may have been processed artificially, such as by excavation, sorting, or haulage	Table A-1
		Basalt	64%	Excavation (general)	Literature	=0= Information based on materials that may have been processed artificially, such as by excavation, sorting, or haulage	Table A-1
		Granite	72%	Excavation (general)	Literature	=0= Information based on materials that may have been processed artificially, such as by excavation, sorting, or haulage	Table A-1
		Sandstone	61%	Excavation (general)	Literature	=0= Information based on materials that may have been processed artificially, such as by excavation, sorting, or haulage	Table A-1
		Slate	77%	Excavation	Literature	=0= Information based on materials that may have been processed artificially, such as by excavation, sorting, or haulage	Table A-1
8	CRWMS M&O (1998)	Welded tuff	20-65% (Elsworth) 15-45% (Gale)	Emplacement drifts	Literature	=1= Information from expert elicitation on potential behavior of emplacement drifts in welded tuff	Direct estimate of Yucca Mountain emplacement drift stability
9	Das (2000)	Sandstone and shale	5%	Longwall coal mining	Volume	=0= Available information suggests this sandstone-shale sequence collapsed, but much of the material did not rubble	Initial value 5%; decreased exponentially with caving height

Table 3-1. Summary of Bulking Factor Information from Literature (continued)

	Reference	Material	Bulking Factor	Context	Method	Relevance Factor and Rationale	Comments
10	Duncan, et al. (1972)	Buckboard Mesa basalt	39–70%	Explosive cratering	Bulk density	=1= Rock type similar to welded tuff. The rubble mechanism may differ somewhat from the mechanism in a degrading emplacement drift.	Blasting fragmentation with some separation in ejecta
11	Duncan, et al. (1980)	Crushed rock	30–56% (compacted)	Rock fill for dam	Porosity	=0= Information based on materials that may have been processed artificially, such as by excavation, crushing, haulage, or compaction	Based on measured porosity of compacted fill
12	Esterhuizen and Karacan (2007)	Sedimentary rock	0–75%	Longwall coal mining	Ratio fall height (h)/block size (b)	=0= Geologic description suggests a rock type that may result in rubble properties different from welded tuff	Correlation between ratio h/b to bulking factor
13	Gilbride, et al. (2005)	Andesite, felsic dikes, and aplite-porphry	9–21% (Goathill) 10% (D Orebody)	Block caving mining	Volume	=1= Geologic description suggests rock types generally similar to welded tuff	Case history of molybdenum mining using block caving; large volume calculation
14	Gilmour and Johnston (1912)	Quartz ore (Waihi, NZ)	40%	Underground mining	Unknown	=0= Geologic description suggests a rock type that may result in rubble properties different from welded tuff	Results quoted in Richards, et al. (2002)
15	Goktepe and Lav (2004)	Surficial deposits	0–40%	Civil earthworks	Volume	=0= Information based on materials that may have been processed artificially, such as by excavation, haulage, or compaction	Values can range up to 100%, but generally less than 40%

Table 3-1. Summary of Bulking Factor Information from Literature (continued)

	Reference	Material	Bulking Factor	Context	Method	Relevance Factor and Rationale	Comments
16	Hartman (1992)	Gneiss	75%	Surface and underground mining	Bulk density	=0= Information provided is insufficient to permit determination of relevance	Table A-2
		Granite	50–86%	Surface and underground mining	Bulk density	=0= Information provided is insufficient to permit determination of relevance	Table A-2
		Granite and porphyry	75%	Surface and underground mining	Bulk density	=0= Information provided is insufficient to permit determination of relevance	Table A-2
		Limestone	65%	Surface and underground mining	Bulk density	=0= Information provided is insufficient to permit determination of relevance	Table A-2
		Sandstone	39–50%	Surface and underground mining	Bulk density	=0= Information provided is insufficient to permit determination of relevance	Table A-2
17	Janach (1976)	Quartzite	2–5%	Compressive testing	Volume	=0= Available information suggests the volumetric expansion resulted from dilational straining under compressive loading, which is different from rubbing	Dilation of individual rock samples at failure
		Mieville granite	14–15%	Punch testing	Volume	=0= Available information suggests the volumetric expansion resulted from dilational straining under compressive loading, which is different from rubbing	Testing on a small volume of rock
		Bohus granite	12–17%	Dynamic compressive loading	Volume	=0= Available information suggests the volumetric expansion resulted from dilational straining under compressive loading, which is different from rubbing	Testing on rock cylinders

Table 3-1. Summary of Bulking Factor Information from Literature (continued)

	Reference	Material	Bulking Factor	Context	Method	Relevance Factor and Rationale	Comments
18	Konak, et al. (2006)	Claystone	47%	Coal mining	Volume	=0= Geologic description suggests a rock type that may result in rubble properties different from welded tuff	Bulking factor back calculated from monitoring data
19	Laubscher (1994)	Fragmented rock	8–16%	Cave mining	Not known	=0= Information could have been based on materials that were processed artificially, such as by excavation, crushing, haulage, or compaction	Based on rock fragmentation; lowest value for coarse fragmentation
20	SNL (2007)	Lithophysal zones in welded tuff	10–40%	Emplacement drifts	Literature	=1= Information determined for Yucca Mountain welded tuff based on literature review	Basis for seismic abstraction for Yucca Mountain
21	Palchik (2002)	Carbonate rock	25–61%	Longwall coal mining	Rock strength	=0= Geologic description suggests a rock type that may result in rubble properties different from welded tuff	Correlation between rock strength and bulking factor
		Weak argillite, sandy shale, and sandstone	8–24%	Underground coal mining	Rock strength and porosity	=0= Geologic description suggests a rock type that may result in rubble properties different from welded tuff	Drifts along coal face; drilling used to determine H/h ratio
22	Pappas and Mark (1993)	Shale	82% (at 0 psi) 27–31% {5.5 MPa [800 psi]}	Longwall coal mining	Lab testing of graded rockfall material	=0= Geologic description suggests a rock type that may result in rubble properties different from welded tuff	Bulking factor dependent on applied load
		Weak sandstone	77% (at 0 psi) 31–34% {5.5 MPa [800 psi]}	Longwall coal mining	Lab testing of graded rockfall material	=0= Geologic description suggests a rock type that may result in rubble properties different from welded tuff	Bulking factor dependent on applied load
		Strong sandstone	86% (at 0 psi) 47–50% {5.5 MPa [800 psi]}	Longwall coal mining	Lab testing of graded rockfall material	=1= Geologic description suggests a rock type generally similar to welded tuff. Data taken as a bulking factor range of 47–86%	Bulking factor dependent on applied load

Table 3-1. Summary of Bulking Factor Information from Literature (continued)							
	Reference	Material	Bulking Factor	Context	Method	Relevance Factor and Rationale	Comments
23	Pappas and Mark (1993)	Shale	14% {5.5 MPa [800 psi]}	Longwall coal mining	Lab testing of uniform rockfall material	=0= Geologic description suggests a rock type that may result in rubble properties different from welded tuff	Bulking factor dependent on applied load and gradation
24	Peele (1961)	Aggregate	14–50%	Placer mining and surface excavation	Volume	=0= Information based on materials that may have been processed artificially, such as by excavation, haulage, or compaction	Clean aggregates bulk less than compact clayey ones
		Various hard rock	66–84%	Hard rock mining	Bulk density	=0= Information provided is insufficient to permit determination of relevance	Based on large rock pieces loaded in mining cars
		Various hard rock	35–48%	Crushed mined hard rock	Bulk density	=0= Information based on materials that may have been processed artificially, such as by excavation, crushing, haulage, or compaction	Based on mixed particle size, slightly shaken
		Solid rock	51–80%	Rock embankments	Volume	=0= Information based on materials that may have been processed artificially, such as by excavation, haulage, or compaction	Large volume structures using various materials

Table 3-1. Summary of Bulking Factor Information from Literature (continued)

	Reference	Material	Bulking Factor	Context	Method	Relevance Factor and Rationale	Comments
25	Peng and Chiang (1984)	Sand	6–15% (original) 1–3% (residual)	Longwall coal mining	Volume	=0= Information based on materials that may have been processed artificially, such as by excavation, haulage, or compaction	Typical values for bulking factor in coal measure rocks
		Clay	<20% (original) 3–7% (residual)	Longwall coal mining	Volume	=0= Geologic description suggests a rock type that may result in rubble properties different from welded tuff	Typical values for bulking factor in coal measure rocks
		Broken coal	<30% (original) 5% (residual)	Longwall coal mining	Volume	=0= Geologic description suggests a rock type that may result in rubble properties different from welded tuff	Typical values for bulking factor in coal measure rocks
		Clay shale	40% (original) 10% (residual)	Longwall coal mining	Volume	=0= Geologic description suggests a rock type that may result in rubble properties different from welded tuff	Typical values for bulking factor in coal measure rocks
		Sandy shale	60–80% (original) 25–35% (residual)	Longwall coal mining	Volume	=0= Geologic description suggests a rock type that may result in rubble properties different from welded tuff	Typical values for bulking factor in coal measure rocks
		Sandstone	50–80% (original) 30–35% (residual)	Longwall coal mining	Volume	=0= Geologic description suggests a rock type that may result in rubble properties different from welded tuff	Typical values for bulking factor in coal measure rocks

Table 3-1. Summary of Bulking Factor Information from Literature (continued)							
	Reference	Material	Bulking Factor	Context	Method	Relevance Factor and Rationale	Comments
26	Peng and Chiang (1984)	Shale	25–30%	Longwall coal mining	Volume	=0= Geologic description suggests a rock type that may result in rubble properties different from welded tuff	Measured rockfall volume
27	Richards, et al. (2002)	Hard rock (quartz andesite), Waihi, NZ	15–50%	Underground mining	Literature	=0= Information derived from literature that is included in this table	Risk assessment of collapse due to caving of mine workings
			15–30%	Open pit mining (stockpile material)	Literature	=0= Information based on materials that may have been processed artificially, such as by excavation, haulage, or compaction	Risk assessment of collapse due to caving of mine workings

Table 3-1. Summary of Bulking Factor Information from Literature (continued)

	Reference	Material	Bulking Factor	Context	Method	Relevance Factor and Rationale	Comments
28	Sweby (1997)	Sandstone and siltstone (coal measure rocks)	5-40%	Longwall coal mining	Borehole measured caving height	=1= Geologic description suggests rock types generally similar to welded tuff	South African mining research on caving mechanisms; large test volume
		Coal	30%	Longwall coal mining	Extensometer measurements	=0= Geologic description suggests a rock type that may result in rubble properties different from welded tuff	South African mining research on caving mechanisms; large test volume
		Silt mudstone	10%	Longwall coal mining	Extensometer measurements	=0= Geologic description suggests a rock type that may result in rubble properties different from welded tuff	South African mining research on caving mechanisms; large test volume
		Carbonaceous shale	15%	Longwall coal mining	Extensometer measurements	=0= Geologic description suggests a rock type that may result in rubble properties different from welded tuff	South African mining research on caving mechanisms; large test volume
		Shale	20%	Longwall coal mining	Extensometer measurements	=0= Geologic description suggests a rock type that may result in rubble properties different from welded tuff	South African mining research on caving mechanisms; large test volume
		Sandy shale	25%	Longwall coal mining	Extensometer measurements	=0= Geologic description suggests a rock type that may result in rubble properties different from welded tuff	South African mining research on caving mechanisms; large test volume
		Shaley sandstone	30%	Longwall coal mining	Extensometer measurements	=1= Geologic description suggests a rock type generally similar to welded tuff	South African mining research on caving mechanisms; large test volume
		Coarse sandstone	40%	Longwall coal mining	Extensometer measurements	=1= Geologic description suggests rock types generally similar to welded tuff	South African mining research on caving mechanisms; large test volume
		Fine sandstone	50%	Longwall coal mining	Extensometer measurements	=1= Geologic description suggests rock types generally similar to welded tuff	South African mining research on caving mechanisms; large test volume

Table 3-1. Summary of Bulking Factor Information from Literature (continued)

	Reference	Material	Bulking Factor	Context	Method	Relevance Factor and Rationale	Comments
29	Trueman (1990)	Coal measure rock	Up to 50%	Coal mining	Literature	=0= Geologic description suggests rock types that may result in rubble properties different from welded tuff	Representative value for United Kingdom coal mines
30	Unrug (1982)	Sedimentary rock	20–50%	Longwall coal mining	Volume	=1= Available information suggests rock types generally similar to welded tuff	Value depends on thickness and fracturing of strata; large test volume
31	Whittaker and Reddish (1989)	Various rock	Up to 50%	Road tunnels	Volume	=0= Available information not sufficient to permit a determination of relevance	Similar mechanism associated with rockfall
32	Wilkinson (1997)	Various soil	5–40%	Civil earthworks	Volume	=0= Information based on materials that may have been processed artificially, such as by excavation, haulage, or compaction	Clay has highest bulking factor; sand and gravel the lowest
		Various rock	50–72%	Civil earthworks	Volume	=0= Information based on materials that may have been processed artificially, such as by excavation, crushing, haulage, or compaction	Strong rock has higher bulking factor than weak rock
33	Yavuz (2004)	Coal measure rock (strong to weak)	21–48%	Coal mining (China)	Rock strength; mined height	=0= Geologic description suggests rock types that may result in rubble properties different from welded tuff	Based on 2.5-m [0.76-ft] mined openings
			24–57%	Coal mining (China)	Rock strength; mined height	=0= Geologic description suggests rock types that may result in rubble properties different from welded tuff	Based on 4.0-m [1.2-ft] mined openings
			48–66%	Coal mining (China)	Rock strength; mined height	=0= Geologic description suggests rock types that may result in rubble properties different from welded tuff	Based on 5.5-m [1.7-ft] mined openings
34	Appendix C	Rubble from Fran Ridge, Yucca Mountain	58–83%	Rubble from lithophysal rock outcrop	Pulled from outcrop manually	=1= Same rock as several emplacement drifts	See Appendix C

DRAFT

cases that provide only one bulking factor value instead of a range of values (e.g., shaley sandstone from item 28 of Table 3-1), these entries were assumed to represent the mean value of a probability distribution with unknown dispersion. For the individual uniform distribution assumption, the effect of these dispersions on the resulting aggregate was tested by varying the range around the mean with a constant value (i.e., $a_i = \mu_i - \xi_i$ and $b_i = \mu_i + \xi_i$). Using this set of assumptions, the range of distributions for the literature and laboratory data subset of 16 is shown in Figure 3-1, where $\xi_i = 5$ percent for all single input data values.

A simple linear-weighted averaging was applied to this set, where the aggregate distribution $f_i(B)$ was derived from the summation $f(B) = \sum w_i f_i(B)$, for $i = 1$ to N (Ayyub, 2001). Because the weight values are equal and constrained to sum up to one, $w_i = 1/N$ for all values within the subset of 16 so that the average can be readily calculated. Linear-weighted averaging results in the aggregate distribution $f(B)$ shown in Figure 3-2(A), along with the corresponding cumulative distribution $F(B)$ in Figure 3-2(B). As expected, the aggregate distribution tends to be skewed toward the values where individual inputs overlap. In both Figures 3-2(A) and 3-2(B), an individual $\xi_i = 5$ percent was also assumed for all the single point values, following the previously described approach. Lognormal and beta distribution fits to $f(B)$ are also shown, derived from the calculated aggregate mean $\mu = 38.4$ percent and standard deviation $\sigma = 19.5$ percent. As shown in Figure 3-2(B), a closer visual fit is observed with the beta distribution, which is also more appropriate to represent some of the bulking factor characteristics (i.e., nonnegative values bounded between 0 and 100 percent). This closer fit can be quantitatively evaluated by comparing the maximum absolute difference between the

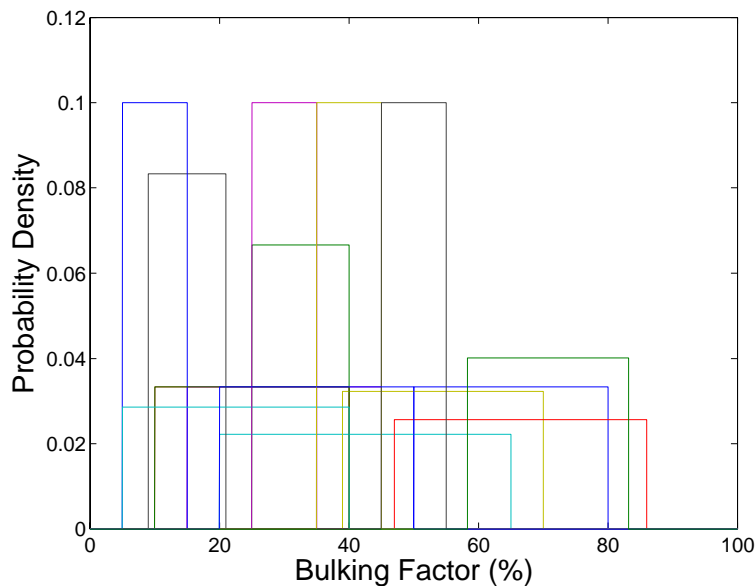
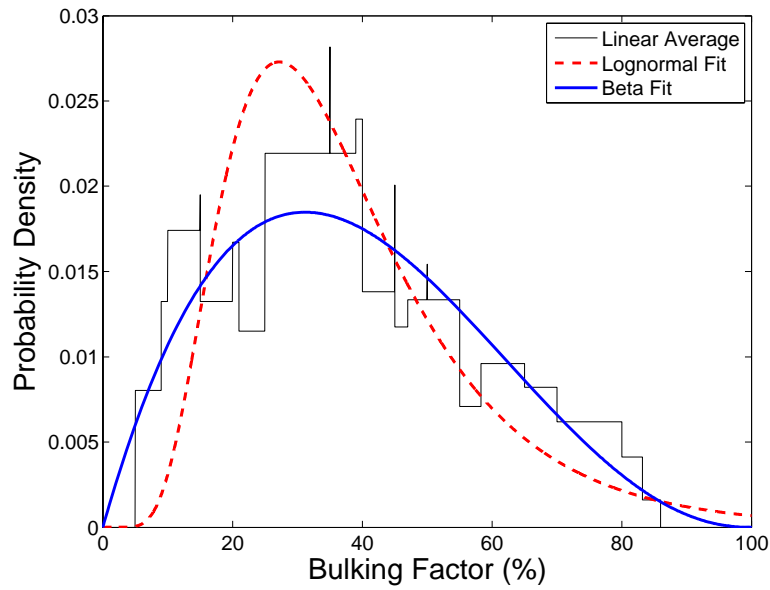
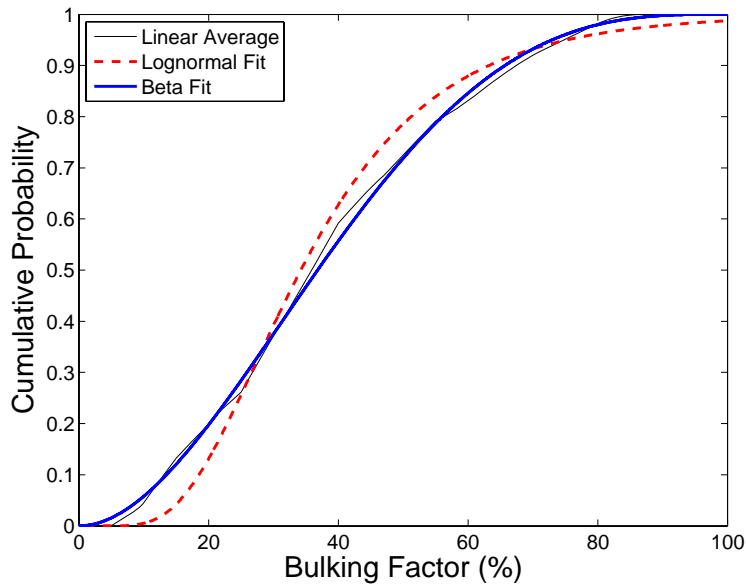


Figure 3-1. Range of Bulking Factor Probability Density Functions for the Subset of 16, Where Each Individual Input Is Represented by a Uniform Probability Density Function With Lower and Upper Limits a_i and b_i , and $\xi_i = 5$ Percent for All Data With One Bulking Factor Value



(A)



(B)

Figure 3-2. Aggregate (A) Probability Density $f(B)$ and (B) Cumulative Distribution $F(B)$ For the Subset of 16 Shown in Figure 3-1 Resulting From a Linear Weighted Average of the Uniformly Distributed Individual $f_i(B)$ Distributions, Including Lognormal and Beta Distributed Fits Based on the Mean μ and Standard Deviation σ of B

DRAFT

aggregate cumulative distribution $F(B)$ and the lognormal $F_{log}(B)$ and beta $F_{beta}(B)$ fits corresponding to the sampled mean and standard deviation of the aggregate. The calculated values of this metric correspond to $\max(|F(B) - F_{beta}(B)|) = 0.04$ and $\max(|F(B) - F_{lognormal}(B)|) = 0.09$ for this case. The corresponding input parameters for the beta distribution shown in Figure 3-2 are $\alpha = 2.0$ and $\beta = 3.2$. Further investigation of the input parameters indicated that increasing the individual ξ_i of the single input values up to 10 percent does not significantly affect the resulting aggregate distribution or the applied beta fit.

The form of the assumed individual probability distributions was also tested by implementing the same approach with normally distributed inputs. In this case, the ranges provided were defined to represent the 5th- and 95th-percentile values (from which mean and standard deviation were derived). For single data, the same approach described previously was used, except the mean for this case was assumed to be that of a normal distribution with unknown spread. The 5th- and 95th-percentile values were assumed to correspond to $\mu_i \pm \xi_i$ for all data with one bulking factor value (with $\xi_i = 5$ percent for all i). Figures 3-3 and 3-4 show the results of this analysis ($\mu = 38.4$ percent and $\sigma = 19.6$, with $\alpha = 2.0$ and $\beta = 3.2$ for a beta distribution fit). Using the metric considered in the previous case to quantify the fit comparison with respect to lognormal and beta distribution results in $\max(|F(B) - F_{beta}(B)|) = 0.03$ and $\max(|F(B) - F_{log}(B)|) = 0.08$, indicating a similar closer fit with the beta distribution. Furthermore, the resulting aggregate distribution does not show significant differences from the uniform distribution assumption described previously. This is expected if the normal and uniform distributions exhibit central tendencies and are similar in terms of dispersion, even if 5th- and 95th-percentile values are used in one case instead of upper and lower bounds. At this stage, no statistical information was collected to indicate that other specific distributions may better reflect the uncertainty in the individual ranges considered. Furthermore, given that the upper and lower values on all the ranges may contain a certain degree of uncertainty, the authors consider the linear average results based on the individual normally distributed assumption to be more appropriate than the results based on the individual uniform distribution assumption. Assuming that each data range represents the 5th- and 95th-percentile bounds allows for the low probability that the actual bulking factor value could lie just outside the range, as opposed to the more stringent assumption that exact bounds are known in the uniform distribution case.

The statistical analysis described in this section indicates that the subset of 16 bulking factor data in Table 3-1 can be represented using a beta distribution with parameters defined in Table 3-2. An equal-weighted analysis of the entire data set without any regard to the assigned relevance factors (i.e., all inclusive) indicates a beta distribution fit can also be used with a mean of 40.0 percent and standard deviation of 21.5 percent, corresponding to $\alpha = 1.7$ and $\beta = 2.5$ [with $\max(|F(B) - F_{beta}(B)|) = 0.03$ and $\max(|F(B) - F_{log}(B)|) = 0.09$]. The close similarity of the two distributions (Figure 3-5) indicates that the distribution described in Table 3-2 can be considered representative of either the subset of 16 or the entire data set. The input data, and therefore the calculated aggregate distribution, represent a wider range of conditions and rock types than could be expected in a degraded emplacement drift. Therefore, the range of bulking factors specific to potential degraded drifts at Yucca Mountain could be narrower than the range represented by the aggregate distribution obtained in this analysis. For example, Sandia National Laboratories (2007) suggests a bulking factor range of 10–40 percent for assessing potential drift degradation, which would represent approximately 50 percent of the probability density area of the beta distribution described in Table 3-2. However, both this range and the CNWRA (2007) bulking factor distribution are encompassed by the distribution determined from the analysis described in this report, as would be expected. Furthermore, as

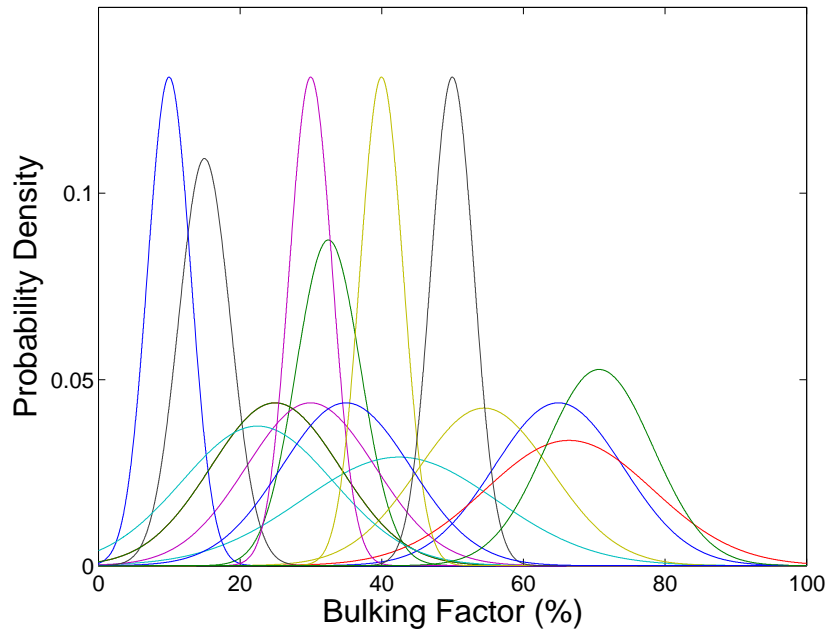


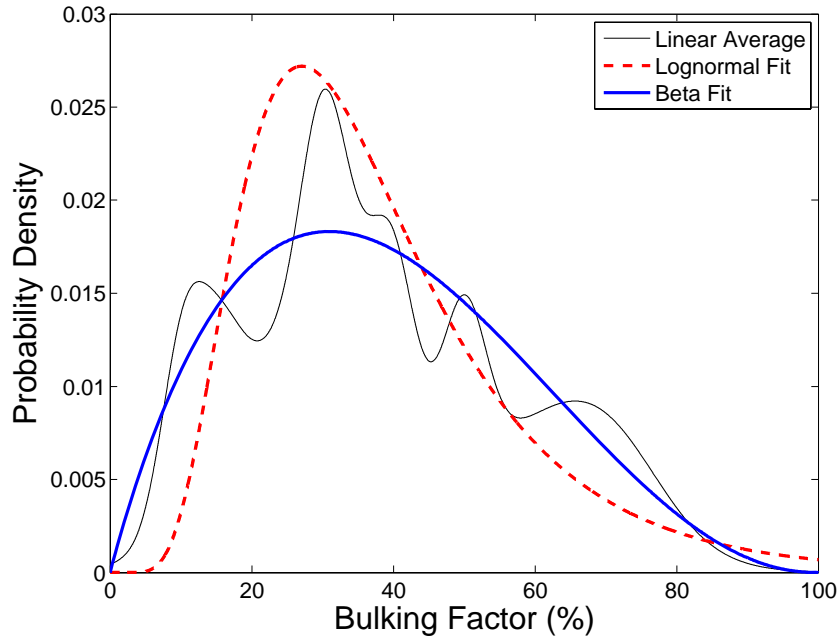
Figure 3-3. Range of Bulking Factor Probability Density Functions for the Subset of 16, Where Each Individual Input Is Represented by a Normal Probability Density Function With 5th- and 95th-Percentile Values Corresponding to $\mu_i \pm \xi_i$ and $\xi_i = 5$ Percent for All Data With One Bulking Factor Value

shown in Figure 3-5, both cover areas of higher probability density (i.e., as opposed to the tailends) within the aggregate distribution fits obtained.

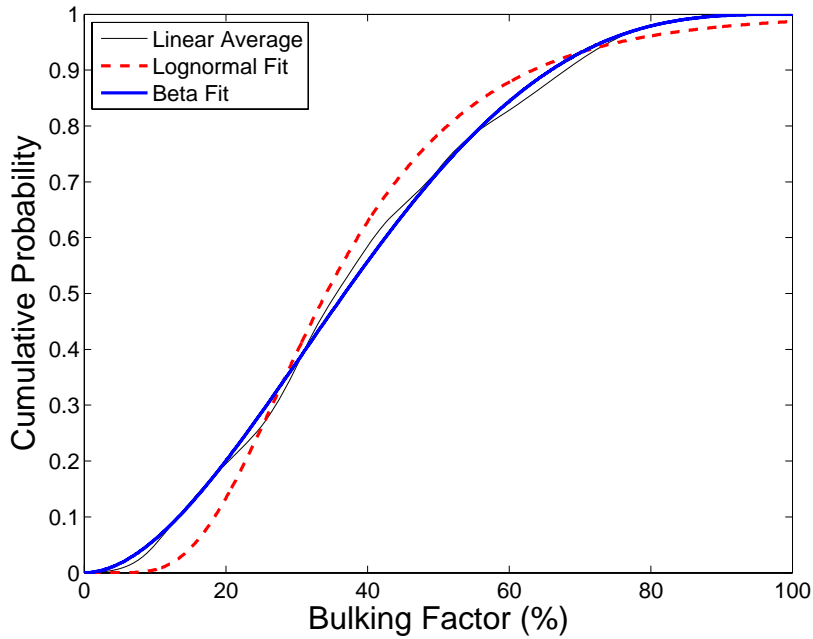
The range of values of bulking factor from laboratory tests described in Appendix C is also indicated in Figure 3-5. The laboratory results suggest a bulking factor in the range of 58–83 percent (Table C–1), which is greater than the 82nd percentile bulking factor from the subset of 16 literature and laboratory data distribution (blue curve in Figure 3-5). As discussed previously in this chapter, important changes to the laboratory procedure would be needed if the procedure were to be used further for bulking factor determination. The needed changes would address the representation of small particle sizes and the effects of gravity compaction in laboratory specimens. Addressing these concerns will likely result in smaller bulking factors as indicated in Appendix C.

The authors recommend using the blue-curve distribution in Figure 3-5 with parameters in Table 3-2 calculated from the subset of 16 literature and laboratory data. The bulking factor distribution input data used for staff analysis with the Total-system Performance Assessment code (CNWRA, 2007) may need to be updated to be consistent with the distribution described in Table 3-2.

DRAFT



(A)



(B)

Figure 3-4. Aggregate (A) Probability Density $f(B)$ and (B) Cumulative Distribution $F(B)$ for the Subset of 16 Shown in Figure 3-3 Resulting From a Linear Weighted Average of the Normally Distributed Individual $f_i(B)$ Distributions, Including Lognormal and Beta Distributed Fits Based on the Mean μ and Standard Deviation σ of B

DRAFT

DRAFT

Table 3-2. Bulking Factor Distribution Derived From the Subset of 16 Literature Data in Table 3-1 Assuming a Beta Distribution Fit		
Bulking Factor, B (Percentage)	Corresponding TPA 5.1a Bulking Factor, B₁	Probability Density Area (Percentage)
B < 10%	B ₁ < 1.1	6.0
10% < B < 60%	1.1 < B ₁ < 1.6	78.4
10% < B < 90%	1.1 < B ₁ < 1.9	93.8
B < 90%	B ₁ < 1.9	99.7
Mean bulking factor = 38.4 percent, standard deviation = 19.6 percent Mean of B ₁ = 1.38, standard deviation = 0.196 Beta distribution parameters: $\alpha = 1.97$, $\beta = 3.2$		

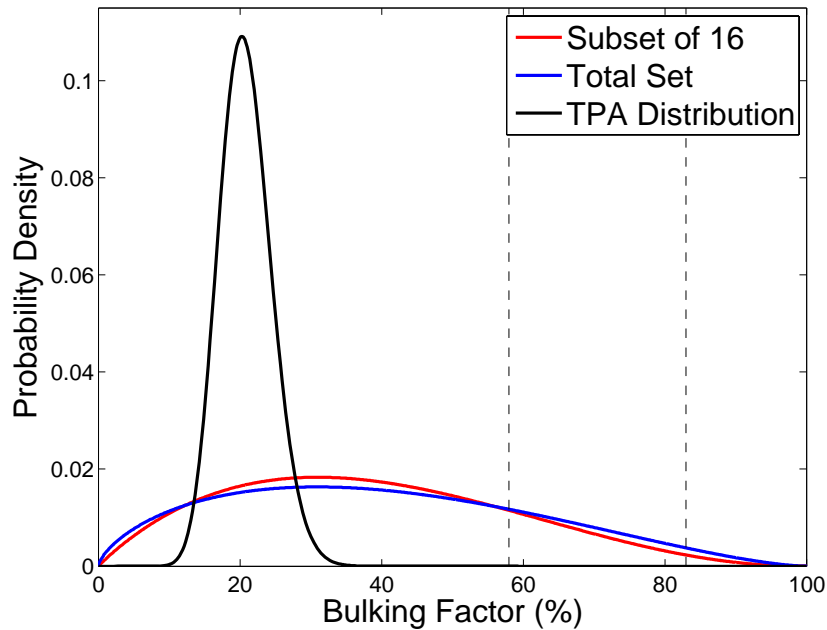


Figure 3-5. Comparison Between the Bulking Factor Probability Densities for the Input Distribution Currently Assumed in the TPA Code and the Aggregate Distribution Fits Based on the Individual Normally Distributed Assumption for the Subset of 16 in Figure 3-3 and the Entire Data Collected From Literature. Dashed Vertical Lines Indicate the Range of Values of Bulking Factor From Laboratory Tests Described in Appendix C.

DRAFT

4 CONCLUSIONS

The literature review identified several factors that affect the bulking behavior of rock, including the following.

- (1) Rock type or lithology affects the grain structure and bonding within intact rock and its propensity to disaggregate during a rockfall event. Less disaggregation may result in poorly sorted rubble with a relatively high bulking factor compared to more disaggregated and better sorted rubble.
- (2) *In-situ* porosity influences the *in-situ* bulk density. If some of the pore spaces of the intact rock collapse when the rock breaks up into rubble, the bulking factor may be smaller than the case of a rock that does not have collapsible void. Collapse of large voids (e.g., lithophysae), therefore, may contribute to smaller bulking factor.
- (3) Particle size distribution influences bulking factor. A poorly sorted material with a more uniform gradation tends to exhibit higher bulking factor than well-sorted material with a distributed gradation covering a range of particle sizes. Bulking factor was shown to be relatively insensitive to the maximum particle size and can be determined using material with a particle gradation of similar shape to the gradation of the target material, but smaller maximum particle size. Fine particles have a large affect on bulking factor as they tend to reduce void volume in rock rubble.
- (4) Particle shape (shape of rock fragments) affects the density of particle packing and hence the bulking factor. Rubble comprising rock fragments with smaller thickness-to-width ratios tends to be more densely packed than rubble made up of more uniformly shaped particles. Denser packing results in lower bulking factor.
- (5) Rock strength affects bulking factor, with stronger, more competent rock having a greater bulking factor than weaker rock where the rubble is in a disorderly arrangement. This trend is partly attributable to the amount of breakage that occurs during rockfall and the resulting particle distribution.
- (6) Rock–mass structure (e.g., joint patterns) affects the size of rock blocks liberated during a rockfall. Depending on the size of blocks relative to the opening dimensions, larger blocks may experience less rotation and disaggregation during rockfall and hence lower bulking factors than smaller blocks. Very large blocks or massive strata may create a stable arch above the opening and limit the amount of material that detaches during a rockfall.
- (7) The fall height of individual blocks affects block rotation, particle arrangement in the resulting rubble, and stress generated in the block on impact. Lower fall height generally results in smaller bulking factor if rotation of larger blocks is limited, but may increase bulking factor by reducing the amount of fines generated from rockfall.
- (8) Vertical stress in the rubble pile affects the bulking factor. For very large accumulations, the stress variation within the rubble pile is likely to result in a nonuniform bulking factor, with lower bulking factors near the bottom of the rubble pile due to gravity loading alone. In cases where the overlying strata deforms to transfer the full weight of the overburden

DRAFT

DRAFT

to the accumulated rubble (e.g., longwall caving), the resulting bulking factors may be very low relative to the initial condition immediately following a rockfall event.

- (9) Vibratory compaction (e.g., from seismic loading) can cause a decrease in bulking factor. The use of compaction equipment in civil engineering applications, for example, reduces bulking factor. Similarly, shaking of material during sieving or screening can also reduce bulking factor significantly. Transportation and stockpiling of material may increase bulking if the final arrangement of rock fragments is more disorderly than the condition immediately following a rockfall. Similarly, production of laboratory-scale samples of rockfall rubble may result in a more disorderly arrangement of fragments, and therefore larger bulking factor.

Although literature information suggests general relationships among bulking factor and several of the factors listed in items 1–9, such as particle shapes, compressive strength, and fall height, the combined effects on bulking factor are in general not sufficiently well understood to be described by analytical expressions that could be used to calculate bulking factor. In addition to the literature review summarized in Table 3-1, this report includes an analysis of limited field data to obtain rubble characteristics such as particle shape and size distributions that could be used to determine bulking factors. However, the information has not been used to determine bulking factors, because of inadequate understanding of the relationships between bulking factor and particle size and shape distributions. The analysis documented in this report focused on using bulking factor information from the literature and limited laboratory testing to obtain a statistical distribution that captures the variability of bulking factor among the reviewed literature. The literature and laboratory data was filtered to obtain data representing rock characteristics and rubble mechanisms similar to conditions that could occur in a degrading underground opening in welded volcanic tuff. Analysis documented in the report suggests that the filtered data retained enough of the statistical characteristics of the unfiltered data, such that a beta distribution fit calculated based on the filtered data can represent either the filtered or unfiltered data.

The authors, therefore, consider the calculated distribution (Table 3-2 and Figure 3-5) as a good representation of bulking factor data from the literature that can be used to study the effects of bulking factor variability on rubble accumulation, drift degradation extent, thermal-hydrological effects of rubble, and the effects of drift degradation on performance of a potential repository at Yucca Mountain. The Total-system performance assessment Version 5.1a input parameters representing bulking factor (CNWRA, 2007) may need to be updated to be consistent with the calculated distribution.

DRAFT

DRAFT

5 REFERENCES

- Ayyub, B.M. *Elicitation of Expert Opinions for Uncertainty and Risks*. 1st Edition. Boca Raton, Florida: CRC Press, LLC. 2001.
- Barczak, T.M. "A Retrospective Assessment of Longwall Roof Support With a Focus on Challenging Accepted Roof Support Concepts and Design Premises." Proceedings of 25th International Conference on Ground Control in Mining, August 1–3, 2006. S.S. Peng, C. Mark, G. Finfinger, S. Tadolini, A.W. Khair, K. Heasley, and Y. Luo, eds. Morgantown, West Virginia: West Virginia University. pp. 232–244. 2006.
- Bechtel SAIC Company, LLC. "Drift Degradation Analysis." ANL–EBS–MD–000027. Rev 03. Las Vegas, Nevada: Bechtel SAIC Company, LLC. 2004.
- Becker, E., C.K. Chan, and H.B. Seed. "Strength and Deformation Characteristics of Rockfill Materials in Plane Strain and Triaxial Compression Tests." Report TE–72–3. Berkely, California: Department of Civil Engineering, University of California-Berkeley. p. 121. 1972.
- Bell, F.G. and R. Stacey. "Subsidence in Rock Masses." *Engineering in Rock Masses*. Jordan Hill, Oxford: Butterworth-Heinemann. 1992.
- Bétournay, M.C. "Rock Mass Displacements and Surface Disruptions Anticipated From Weak Rock Masses of Metal Mines." Presented at Interstate Technical Group on Abandoned Underground Mines, 5th Biennial Workshop, Tucson, Arizona, April 21–23, 2004. <[www.azdot.gov/Highways/Materials/Geotech Design/Seminar/](http://www.azdot.gov/Highways/Materials/Geotech%20Design/Seminar/)>
- _____. "Underground Mining and Its Surface Effects." Presented at Interstate Technical Group on Abandoned Underground Mines, 4th Biennial Workshop, Illinois Department of Transportation, Davenport, Iowa, May 1–3, 2002. Davenport, Iowa: The Iowa Department of Transportation and the Illinois Department of Transportation. 2002.
- Blyth, F.G.H. and M.H. de Freitas. *A Geology for Engineers*. Jordan Hill, Oxford: Edward Arnold. 1990.
- Brady, B.H.G. and E.T. Brown. *Rock Mechanics For Underground Mining*. 3rd Edition. Boston, Massachusetts: Kluwer Academic Publishers. p. 628. 2004.
- Brzovica, A. and E. Villaescusa. "Rock Mass Characterization and Assessment of Block-Forming Geological Discontinuities During Caving of Primary Copper Ore at the El Teniente Mine, Chile." *International Journal of Rock Mechanics & Mining Sciences*. Vol. 44. pp. 565–583. 2007.
- Church, H.K. *Excavation Handbook*. New York City, New York: McGraw-Hill. 1981.
- CNWRA. "Total-system Performance Assessment (TPA) Version 5.1a." San Antonio, Texas: CNWRA. September 2007.

DRAFT

DRAFT

CRWMS M&O. "Near-field/Altered Zone Coupled Effects Expert Elicitation Project."
Las Vegas, Nevada: CRWMS M&O. MOL.19980729.0638. 1998.
<<http://domino.ymp.gov/va/support/nfazceep.nsf/>> (January 15, 2008).

Das, S.K. "Observations and Classification of Roof Strata Behaviour Over Longwall Coal Mining Panels in India." *International Journal of Rock Mechanics and Mining Sciences*. Vol. 37, No. 4. pp 585–597. 2000.

DOE. "Yucca Mountain Science and Engineering Report: Technical Information Supporting Site Recommendation Consideration." Report DOE/RW-0539. Washington, DC: DOE, Office of Civilian Radioactive Waste Management. 2001.

Duncan, J.M., P.A. Witherspoon, J.K. Mitchell, D.J. Watkins, J.H. Hardcastle, and J.C.Chen. "Seepage and Groundwater Effects Associated with Explosive Cratering: Department of Civil Engineering." Report No. TE-72-2. Berkeley, California: University of California. p. 190. 1972.

Duncan, J.M., P. Byrne, K.S. Wong, and P. Mabry. "Strength, Stress-Strain and Bulk Modulus Parameters for Finite Element Analyses of Stresses and Movements in Soil Masses." UCB/GT/80-01. Berkeley, California: University of California, College of Engineering, Office of Research Services. 1980.

Dunrud, C.R. "Engineering Geology Applied to the Design and Operation of Underground Coal Mines." Bulletin 2147. Washington, DC: U.S. Geological Survey. p. 134. 1998.

Esterhuizen, G.S. and C.O. Karacan. "A Methodology for Determining Gob Permeability Distributions and Its Application to Reservoir Modeling of Coal Mine Longwalls." 2007 SME Annual Meeting and Exhibit, Denver, Colorado, February 25–28, preprint 07-78. NIOSHTIC-2 No. 20031652. Littleton, Colorado: Society for Mining, Metallurgy, and Exploration, Inc. 2007.

Ferm, J.C. and G.C. Smith. "A Guide to Cored Rocks in the Pittsburgh Basin." Lexington, Kentucky: Department of Geology; University of South Carolina; Columbia, South Carolina: University of Kentucky. pp. 109. 1980.

Franklin, J.A., N.H. Maerz, and C.P. Bennet. "Rock Mass Characterization Using Photoanalysis." *International Journal of Mining and Geology*. Vol. 6. pp. 97–112. 1988.

Fumagalli, E. "Test on Cohesionless Material for Rockfill Dams." *Journal of Soil Mechanics and Foundation Division*. Vol. 95, No. SM1. pp. 313–330. 1969.

Gilbride, L.J., K.S. Free, and R. Kehrman. "Modeling Block Cave Subsidence at the MolyCorp, Inc., Questa Mine—A Case Study." Paper ARMA/USRMS 05-881. Presented at Alaska Rocks 2005, 40th U.S. Symposium on Rock Mechanics (USRMS): Rock Mechanics for Energy. Mineral and Infrastructure Development in the Northern Regions, Anchorage, Alaska, June 25–29, 2005. Anchorage, Alaska: Terralog Technologies, Inc. 2005.

Gilmour, J.L. and W.H. Johnston. "Mining Methods in the Waihi Mine, New Zealand." *Transactions of the Australasian Institute of Mining Engineers*. Vol 16. pp. 26–52. 1912.

Goktepe, A.B. and A.H. Lav. "Method for Optimizing Earthwork Considering Soil Properties in The Geometric Design of Highways." Vol. 130, No 4. pp. 183–190. 2004.

DRAFT

DRAFT

Hartman, H.L., ed. *SME Mining Engineering Handbook*. 2nd Edition. Vol. 2. Littleton, Colorado: Society for Mining, Metallurgy and Exploration, Inc. 1992.

Janach, W. "The Role of Bulking in Brittle Failure of Rocks Under Rapid Compression." *International Journal of Rock Mechanics Mining and Science & Geomechanics*. Abstract Vol. 13. pp. 177–186. 1976.

Konak, G., T. Onargan, C.O. Aksoy, H. Kose, C. Tatar, and C. Pamukcu. "Determination of Immediate Roof at Mines of the Kutahya-Omerler Coal Basin, Turkey." *Journal of Mining Science*. Vol. 42, No. 2. pp 157–170. 2006.

Laubscher, D.H. "Cave Mining—State of the Art." *Journal of the South African Institute of Mining and Metallurgy*. Vol. 94, No. 10. pp. 279–293. 1994.

Marachi, N.D., C.K. Chan, H.B. Seed, and J.M. Duncan. "Strength and Deformation Characteristics of Rockfill Materials." Report TE-69–5. Berkeley California: Department of Civil Engineers, University of California Berkeley. pp. 139. 1969.

Munson, D.E. and S.E. Benzley. "Analytic Subsidence Model Using Void-Volume Distribution Functions." 21st US Rock Mechanics Symposium. Vol. 69, No. 5. Rolla, Missouri: Seismological Society of America. pp. 1,643–1,644, 1980.

Ofoegbu, G., R. Fedors, C. Grossman, S. Hsiung, L. Ibarra, C. Manepally, J. Myers, M. Nataraja, O. Pensado, K. Smart, and D. Wyrick. "Summary of Current Understanding of Drift Degradation and Its Effects on Performance at a Potential Yucca Mountain Repository." Rev. 1. CNWRA 2006-02. San Antonio, Texas: CNWRA. January 2007.

Nelson, A. *Dictionary of Mining*. New York City, New York: Philosophical Library Inc. 1965.

Palchik, V. "Influence of Physical Characteristics of Weak Rock Mass on Height of Caved Zone Over Abandoned Subsurface Coal Mines." *Environmental Geology*. Vol. 42. pp. 92–101. 2002.

Pappas, D.M. and C. Mark. "Behavior of Simulated Gob Material." Report of Investigations RI 9458. 1993.

Peele, R. *Mining Engineers' Handbook*. 3rd Edition. New York City, New York: John Wiley & Sons. 1961.

Peng, S.S. and H.S. Chiang. *Longwall Mining*. New York City, New York: John Wiley & Sons. 1984.

Richards, L., C. Mazengarb, D. Beetham, B. Brathewaite, and W. Smith. "Waihi Underground Mine Workings, Stage II Investigations (Risk Assessment and Mitigation)." August 2002. Report by Institute of Geological and Nuclear Sciences Ltd. To Hauraki District Council Vol. 1. <www.hauraki-dc.govt.nz/news/Mining-issues/mineworkingsreport/MineReport/>

Salamon, M.D.G. "Mechanism of Caving in Longwall Coal Mining." *In Rock Mechanics Contributions and Challenges: Proceedings of the 31st U.S. Symposium*. Golden, Colorado. Balkema: Rotterdam: pp. 161–168. 1990.

DRAFT

DRAFT

Sandia National Laboratories. "Seismic Consequence Abstraction." Report MDL-WIS-PA-000003. Rev 03. DOC-20070928.0011. Livermore, California: Sandia National Laboratories. 2007.

Sweby, G. "Review the Caving Mechanisms Around High Extraction Systems and Determine the Effect of the Mechanisms on the Safety of the System." CSIR Miningtek Project No. COL-327, October 1997. Submitted to Safety in Mines Research Advisory Committee (SIMRAC). October 1997.

Telford, W.M., L.P. Geldart, R.E. Sheriff, and D.A. Keys. *Applied Geophysics*. Cambridge, Massachusetts: Cambridge University Press. 1976.

Trueman, R. "A Finite Element Analysis for the Establishment of Stress Development in a Coal Mine Caved Waste." *Mining Science of Technology*. Vol. 10. pp. 247-252. 1990.

Unrug, K.F. "Roof Falls and Caving in Longwall Mining Operations." *In Proceedings of the 2nd Conference on Ground Control in Mining*. Morgantown, West Virginia: Department of Mining Engineering, West Virginia University. pp. 45-52. 1982.

Wang, L.G., S. Yamashita, F. Sugimoto, C. Pan, and G. Tan. "A Methodology for Predicting the *In-Situ* Size and Shape Distribution of Rock Blocks." *Rock Mechanics and Rock Engineering*. Vol. 36, No. 2. pp. 121-142. 2003.

Whittaker, B.N. and D.J. Reddish. *Subsidence-Occurrence, Prediction and Control*. Amsterdam, Netherlands: Elsevier, Amsterdam. 1989.

Wilkinson, D. "WWW Pages for Road Design." MEng final year project report. University of Durham: Durham, United Kingdom : School of University of Durham. p. 42. 1997.

Yavuz, H. "An Estimation Method for Cover Pressure Re-Establishment Distance and Pressure Distribution in the Goaf of Longwall Coal Mines." *International of Journal Rock Mechanics and Mining Sciences*. Vol. 41. pp. 193-205. 2004.

DRAFT

DRAFT

APPENDIX A

DRAFT

DRAFT

ESTIMATED BULKING FACTORS FOR GEOLOGIC MATERIALS

Table A-1. Approximate Material Characteristics*						
Material	<i>In-situ</i>		Loose Condition		Fill Condition	
	Specific Gravity	Bulk Density (kg/m³)†	Swell (Percentage)	Bulk Density (kg/m³)†	Swell or Shrink (Percentage)	Bulk Density (kg/m³)†
Adobe, S	(1.91)	1,917	35	1,413	-10	2,119
Andesite, I	2.94	2,938	67	1,763	33	2,214
Asbestos	2.40	2,398	67	1,436	—	—
Ashes, coal	(0.61)	611	33	475	-50	1,223
Asphaltum, S	1.28	1,276	67	825	—	—
Asphalt rock, S	2.41	2,404	62	1,484	—	—
Aragonite, calcium ore‡	3.00	2,997	67	1,792	—	—
Argentite, silver ore‡	7.31	7,301	67	4,368	—	—
Barite, barium ore‡	4.48	4,487	67	2,683	—	—
Basalt, I	2.94	2,938	64	1,792	36	2,160
Bauxite, aluminum ore‡	2.73	2,623	50	1,745	—	—
Bentonite	1.60	1,603	35	1,187	—	—
Biotite, mica ore‡	2.88	2,879	67	1,721	—	—
Borax, S	1.73	1,733	75	991	—	—
Breccia, S	2.41	2,404	33	1,804	27	1,893
Calcite, calcium ore‡	2.67	2,671	67	1,603	—	—
Caliche, S	(1.44)	1,442	16	1,246	-25	1,899
Carnotite, uranium ore‡	2.47	2,463	50	1,644	—	—
Cassiterite, tin ore‡	7.17	6,755	67	4,036	—	—
Cement	—	—	—	1,603	—	—
Cerrusite, lead ore‡	6.50	6,511	67	3,894	—	—
Chalcocite, copper ore‡	5.70	5,698	67	3,413	—	—
Chalcopyrite, copper ore‡	4.20	4,190	67	2,505	—	—
Chalk, S	2.42	2,410	50	1,608	33	1,810
Charcoal	—	—	—	611	—	—
Chat, mine tailings	—	—	—	1,603	—	—
Cinders	(0.76)	760	33	570	-10	843
Cinnabar, mercury ore‡	8.10	8,090	67	4,849	—	—
Clay, S:						
Dry	(1.91)	1,911	35	1,413	-10	2,119
Damp	(1.99)	1,988	40	1,425	-10	2,208
Clinker	—	—	—	1,525	—	—
Coal, S:						
Anthracite	1.55	1,549	70	908	—	—
Bituminous	1.35	1,353	67	813	—	—
Coke	(0.51)	510	0	510	—	—
Colemanite, borax ore‡	1.73	1,733	75	991	—	—

DRAFT

Table A-1. Approximate Material Characteristics* (continued)

Material	<i>In-situ</i>		Loose Condition		Fill Condition	
	Specific Gravity	Bulk Density (kg/m ³)†	Swell (Percentage)	Bulk Density (kg/m ³)†	Swell or Shrink (Percentage)	Bulk Density (kg/m ³)†
Concrete:						
Stone	2.35	2,350	72	1,371	33	1,727
Cyclopean	2.48	2,481	72	1,442	33	1,870
Cinder	1.76	1,763	72	1,027	33	1,330
Conglomerate, S	2.21	2,208	33	1,662	-8	2,392
Decomposed rock:						
75% Rock, 25% Earth	(2.45)	2,445	25	1,959	12	2,196
50% Rock, 50% Earth	(2.23)	2,226	29	1,721	-5	2,339
25% Rock, 75% Earth	(2.01)	2,006	26	1,579	-8	2,184
Diabase, I	3.00	2,997	67	1,787	33	2,261
Diorite, I	3.10	3,098	67	1,858	33	2,333
Diatomite, S:						
Diatomaceous earth	(0.87)	873	62	540	—	—
Dolomite, S	2.88	2,891	67	1,727	43	2,018
Earth, loam, S:						
Dry	(1.84)	1,798	35	1,330	-12	2,089
Damp	(2.00)	2,000	40	1,425	-4	2,089
Wet, mud	(1.75)	1,745	0	1,745	-20	2,089
Earth-rock mixtures:						
75% Earth, 25% Rock	(2.01)	2,006	26	1,579	-8	2,184
50% Earth, 50% Rock	(2.23)	2,226	29	1,721	-5	2,339
25% Earth, 75% Rock	(2.45)	2,445	25	1,959	12	2,196
Feldspar, I	2.62	2,618	67	1,567	33	1,971
Felsite, I	2.50	2,499	67	1,496	33	1,882
Fluorite, S	3.10	3,098	67	1,858	—	—
Gabbro, I	3.10	3,098	67	1,858	33	2,339
Galena, lead ore‡	7.51	7,496	67	4,493	—	—
Gneiss, M	2.71	2,701	67	1,614	33	2,030
Gob, mining refuse	(1.75)	1,745	0	1,745	-20	2,089
Gravel, average graduation, S:						
Dry	(1.79)	1,792	15	1,549	-7	1,923
Wet	(2.09)	2,095	5	1,988	-3	2,160
Granite, I	2.69	2,695	72	1,567	33	2,024
Gumbo, S:						
Dry	(1.91)	1,917	50	1,276	-10	2,119
Wet	(1.99)	1,988	67	1,199	-10	2,208
Gypsum, S	2.43	2,422	72	1,413	—	—
Hematite, iron ore‡	5.08	5,081	75	2,896	—	—
Hessite, silver ore‡	8.50	8,488	67	5,081	—	—
Ice	0.93	926	67	552	—	—
Ilmenite, titanium ore‡	4.75	4,748	69	2,807	—	—
Kaolinite, S:						
Dry	(1.91)	1,917	50	1,276	—	—
Wet	(1.99)	1,988	67	1,193	—	—

DRAFT

DRAFT

Table A-1. Approximate Material Characteristics* (continued)

Material	<i>In-situ</i>		Loose Condition		Fill Condition	
	Specific Gravity	Bulk Density (kg/m ³)†	Swell (Percentage)	Bulk Density (kg/m ³)†	Swell Or Shrink (Percentage)	Bulk Density (kg/m ³)†
Ignite	(1.25)	1,246	65	754	—	—
Limestone, S	2.61	2,600	63	1,597	36	1,911
Linnaeite, cobalt ore‡	4.89	4,885	67	2,926	—	—
Limonite, iron ore‡	3.80	3,799	55	2,457	—	—
Loam, earth, S:						
Dry	(1.84)	1,798	35	1,330	-12	2,089
Damp	(2.00)	2,000	40	1,425	-4	2,089
Wet, Mud	(1.75)	1,745	0	1,745	-20	2,089
Loess, S:						
Dry	(1.91)	1,911	35	1,413	-10	2,119
Wet	(1.99)	1,988	40	1,425	-10	2,208
Magnesite, magnesium ore‡	3.00	2,997	50	1,994	—	—
Magnetite, iron ore‡	5.04	5,027	54	3,276	—	—
Marble, M	2.68	2,683	67	1,603	33	2,018
Marl, S	2.23	2,220	67	1,330	33	1,674
Masonry, rubble	2.33	2,327	67	1,395	33	1,751
Millerite, nickel ore‡	5.65	5,656	67	3,389	—	—
Molybdenite, molybdenum ore‡	4.70	4,695	67	2,819	—	—
Mud, S	(1.75)	1,745	0	1,745	-20	2,089
Muscovite, mica ore‡	2.89	2,885	67	1,727	—	—
Niccolite, nickel ore‡	7.49	7,479	67	4,481	—	—
Orpiment, arsenic ore‡	3.51	3,502	50	2,339	—	—
Pavement:						
Asphalt	1.93	1,923	50	1,151	0	1,923
Brick	2.41	2,404	67	1,442	33	1,810
Concrete	2.35	2,350	67	1,407	33	1,769
Macadam	1.69	1,686	67	1,009	0	1,686
Wood block	0.97	967	72	564	33	724
Peat	(0.70)	700	33	528	—	—
Phosphorite, phosphate rock, S	3.21	3,205	50	2,137	—	—
Porphyry, I	2.74	2,748	67	1,644	33	2,066
Potash, S	2.20	2,196	50	1,466	—	—
Pumice, I	0.64	641	67	386	—	—
Pyrites, iron ore‡	5.07	5,069	67	3,033	—	—
Pyrolusite, manganese ore‡	4.50	4,487	50	2,997	—	—
Quartz, I	2.59	2,588	67	1,549	33	1,947
Quartzite, M	2.68	2,683	67	1,608	33	2,018
Realgar, arsenic ore‡	3.51	3,502	50	2,333	—	—
Rhyolite, I	2.40	2,404	67	1,436	33	1,804
Riprap rock, average	2.67	2,671	72	1,549	43	1,870
Rock-Earth Mixtures:						
75% Rock, 25% Earth	(2.45)	2,445	25	1,959	12	2,196

DRAFT

DRAFT

Table A-1. Approximate Material Characteristics* (continued)

Material	In-situ		Loose Condition		Fill Condition	
	Specific Gravity	Bulk Density (kg/m ³)†	Swell (Percentage)	Bulk Density (kg/m ³)†	Swell Or Shrink (Percentage)	Bulk Density (kg/m ³)†
50% Rock, 50% Earth	(2.23)	2,226	29	1,721	-5	2,339
25% Rock, 75% Earth	(2.01)	2,006	26	1,579	-8	2,184
Salt, rock, S	2.18	2,178	67	1,306	—	—
Dry	(1.71)	1,709	11	1,537	-11	1,923
Wet	(1.84)	1,834	5	1,917	-11	2,054
Sandstone, S	2.42	2,416	61	1,496	34	1,798
Scheelite, tungsten ore‡	5.98	5,995	67	3,591	—	—
Schist, M	2.59	2,689	67	1,608	33	2,024
Serpentine, asbestos ore‡	2.62	2,635	67	1,573	—	—
Shale, S	2.64	2,641	50	1,763	33	1,988
Silt, S	(1.93)	1,923	36	1,413	-17	2,309
Siltstone, S	2.42	2,416	61	1,496	-11	2,707
Slag:						
Furnace	2.87	2,873	98	1,597	65	1,739
Sand	(0.83)	831	11	748	-11	932
Slate, M	2.68	2,671	77	1,543	33	2,006
Smaltite, cobalt ore‡	6.48	6,511	67	3,894	—	—
Snow:						
Dry	(0.13)	131	0	131	—	—
Wet	(0.51)	510	0	510	—	—
Soapstone, talc ore‡	2.70	2,701	67	1,614	—	—
Sodium niter, chile saltpeter	2.20	1,608	50	1,466	—	—
Stibnite, antimony ore‡	4.58	4,576	67	2,736	—	—
Sulfur	2.00	2,048	50	1,371	—	—
Syenite, I	2.64	2,647	67	1,585	33	1,988
Taconite, iron ore‡	3.18	3,187	60	1,994	—	—
Talc, M	2.70	2,754	67	1,650	33	2,071
Topsoil, S	(1.44)	1,442	56	962	-26	1,947
Trachyte, I	2.40	2,404	67	1,436	33	1,810
Trap rock, igneous rocks, I	2.79	2,796	67	1,674	33	2,101
Trash	—	—	—	237	-50	475
Tuff, S	2.41	2,404	50	1,603	33	1,810
Witherite, barium ore‡	4.29	4,291	67	2,564	—	—
Wolframite, tungsten ore‡	7.28	7,289	67	4,363	—	—
Zinc blende, zinc ore‡	4.02	4,024	67	2,410	—	—
Zincite, zinc ore‡	5.68	5,668	67	3,389	—	—

*Church, H.K. *Excavation Handbook*. New York City, New York: McGraw-Hill. 1981.

†1 kg/m³ = 0.0624 lb/ft³

‡Ores in the mineral state without gangues.

Notes:

I—Igneous rock. S—Sedimentary rock. M—Metamorphic rock.

()—Apparent specific gravity as material is not solid.

Bulk densities provided by Church (1981) are subject to an average ±10 percent variation.

Swell and shrinkage factors are subject to an average ±33 percent variation for both rock and earth materials.

Church (1981) assigned a loose-state swell factor of 67 percent and compacted-state swell factor of 33 percent to any rock for which he had no swell factor information.

DRAFT

DRAFT

Table A-2. Approximate Material Characteristics*						
Material	<i>In-Situ</i> Bulk Density (kg/m³)		Loose Bulk Density (kg/m³)		Bulking Factor (Percentage)	
	Low	High	Low	High	Low	High
Alumina	—	—	961	961	—	—
Ammonium nitrate	—	—	721	721	—	—
Asbestos ore	—	—	1,297	1,297	—	—
Ashes, dry	—	—	561	641	—	—
Ashes, wet	—	—	721	801	—	—
Bauxite, ground, dry	—	—	1,089	1,089	—	—
Bauxite, run of mine	1,602	2,563	1,201	1,922	33	33
Bauxite, crushed, 3 × 0 in	—	—	1,201	1,362	—	—
Clay, compact, natural bed	1,746	1,746	1,313	1,313	33	33
Clay, dense, tough or wet	1,778	1,778	1,329	1,329	34	34
Clay, dry	1,362	1,362	1,089	1,089	25	25
Clay, dry excavated	1,105	1,105	—	—	—	—
Clay, dry in lump, loose	—	—	961	1,121	—	—
Clay, fines	—	—	1,602	1,922	—	—
Clay, light (kaolin)	1,666	1,666	1,281	1,281	30	30
Clay and gravel, dry	1,602	1,602	1,137	1,137	41	41
Clay and gravel, wet	1,826	1,826	1,297	1,297	41	41
Chrome ore	—	—	2,002	2,243	—	—
Cinders, coal	—	—	641	721	—	—
Coal, anthracite	1,297	1,362	961	1,009	35	35
Coal, anthracite, sized	—	—	881	961	—	—
Coal, bituminous	1,121	1,121	801	833	35	40
Coal, bituminous, mined, sized	—	—	721	881	—	—
Coal, bituminous, mined, run-of-mine	—	—	721	881	—	—
Coal, bituminous, mined, slack, 1/2 in and under	—	—	689	801	—	—
Coal, bituminous, strip, not cleaned	—	—	801	961	—	—
Coal, lignite	—	—	641	721	—	—
Coke	—	—	384	497	—	—
Coke, breeze, 1/4 in and under	—	—	400	545	—	—
Coke, loose	—	—	368	561	—	—
Coke, petroleum	—	—	561	641	—	—
Copper ore	—	—	1,602	2,563	—	—
Earth, dry	—	—	913	1,329	—	—
Earth, dry, loam	—	—	913	1,089	—	—
Earth, moist	—	—	1,201	1,362	—	—
Earth, wet	—	—	1,602	1,666	—	—
Earth, wet, containing clay	—	—	1,602	1,762	—	—
Earth, sand, gravel	—	—	1,570	1,570	—	—
Earth, rock	1,490	1,906	1,137	1,458	31	31
Feldspar, 1/2 in screenings	—	—	1,121	1,362	—	—

DRAFT

Table A-2. Approximate Material Characteristics* (continued)

Material	In-Situ Bulk Density (kg/m ³)		Loose Bulk Density (kg/m ³)		Bulking Factor (Percentage)	
	Low	High	Low	High	Low	High
Feldspar, 1 1/2 to 3 in			1,442	1,602		
Feldspar, 200 mesh	—	—	1,602	1,602	—	—
Gneiss	2,691	2,691	1,538	1,538	75	75
Granite	2,675	2,675	1,442	1,778	50	86
Granite and porphyry	2,723	2,723	1,554	1,554	75	75
Graphite ore	—	—	1,041	1,201	—	—
Gravel, run-of-bank	—	—	1,442	1,602	—	—
Gravel, dry	1,458	1,922	737	1,714	12	98
Gravel, dry, screened	—	—	1,442	1,602	—	—
Gravel, wet	2,307	2,307	2,098	2,098	10	10
Gypsum	2,611	2,675	1,602	1,778	50	63
Gypsum, 1/2 in screenings	—	—	1,121	1,281	—	—
Gypsum, 1 1/2 to 3 in	—	—	1,121	1,281	—	—
Iron ore	—	—	1,602	3,204	—	—
Iron ore pellets	—	—	1,858	2,082	—	—
Iron ore, hematite	3,860	5,158	2,307	2,323	67	122
Iron ore, taconite	2,403	3,204	1,714	2,291	40	40
Kaolin	1,666	1,666	1,281	1,281	30	30
Lead ore	—	—	3,204	4,325	—	—
Lime, pebble	—	—	849	897	—	—
Limestone	2,611	2,611	1,586	1,586	65	65
Limestone, blasted	2,499	2,499	1,426	1,490	68	75
Limestone, crushed	—	—	1,362	1,442	—	—
Limestone, marble	2,723	2,723	1,554	1,618	68	75
Manganese ore	—	—	2,002	2,243	—	—
Mud, dry	1,281	1,762	1,057	1,458	21	21
Mud, wet	1,762	2,082	1,458	1,730	20	21
Nickel-cobalt sulfate ore	—	—	1,281	2,403	—	—
Rock, crushed	—	—	2,002	2,323	—	—
Rock, well blasted	2,371	2,371	1,586	1,586	49	49
Rock, soft, excavated with shovel	—	—	1,602	1,762	—	—
Rock, stone, crushed	1,922	2,323	1,426	1,714	35	36
Sand, bank, damp	—	—	1,682	2,082	—	—
Sand, bank, dry	—	—	1,442	1,762	—	—
Sand, dry	1,297	2,018	1,121	1,842	10	16
Sand, moist	2,018	2,018	1,762	1,762	15	15
Sand and gravel, dry	1,970	1,970	1,730	1,730	14	14
Sand and gravel, wet	2,307	2,307	2,002	2,002	15	15
Sandstone	2,307	2,451	1,538	1,762	39	50
Sandstone, broken	—	—	1,362	1,442	—	—
Shale, broken	—	—	1,442	1,602	—	—
Shale, crushed	—	—	1,362	1,442	—	—
Shale, riprap	1,666	1,666	1,249	1,249	33	33

DRAFT

DRAFT

Table A-2. Approximate Material Characteristics* (continued)						
Material	<i>In-Situ</i> Bulk Density (kg/m³)		Loose Bulk Density (kg/m³)		Bulking Factor (Percentage)	
	Low	High	Low	High	Low	High
Slag	2,178	2,178	1,762	1,762	24	24
Slate	2,723	2,883	2,098	2,227	29	30
Stone, crushed	1,922	2,323	1,426	1,714	35	36
Sulphur ore	—	—	1,394	1,394	—	—
Trap rock	2,963	2,963	1,954	1,986	49	52
Zinc ore, crushed	—	—	2,563	2,563	—	—
<p>*Hartman, H.L., ed. <i>SME Mining Engineering Handbook</i>. 2nd Edition. Vol. 2. Littleton, Colorado: Society for Mining, Metallurgy and Exploration, Inc. 1992.</p> <p>Notes: Values given in table may vary considerably from those experienced in the field.</p>						

DRAFT

APPENDIX B

DRAFT

DRAFT

SUMMARY OF FRACTURE AND RUBBLE CHARACTERIZATION FROM LITHOPHYSAL TUFF AT THE SOUTH END OF FRAN RIDGE, YUCCA MOUNTAIN, NEVADA

B.1 INTRODUCTION

The nature and characteristics of rubble that may result from degradation of emplacement drifts in welded lithophysal rocks have not been determined. Spalling of rock during the drift scale heater test and fragments found in the mesh and on the invert in the Exploratory Studies Facility (ESF)¹ tunnel and enhanced characterization of repository block (ECRB)² cross-drift provide qualitative information on the size and shape of fragments. More detailed and quantitative information on rubble characteristics is not available at these locations, however. The size and shape distributions of the fragments and their packing in rubble piles are needed to conceptualize and quantify the flow of water (liquid and gas phase) and heat transfer (conduction, convection, and radiation) for determining the evolution of in-drift environments used in performance assessments of a potential repository. In addition, an understanding of the fragment sizes and shapes and their packing could help constrain estimates of bulking factors, which influence drip shield and waste package performance.

Surface exposures of the Topopah Spring welded Lower Lithophysal zone (Ttptll)³ at the south end of Fran Ridge, Yucca Mountain, were identified as an analog site to the host rock that would enable detailed fracture characterization and collection of rubble samples (Smart and Fedors, 2006). The objective was to obtain a more quantitative understanding of rubble size distributions by examining fractured outcrops of lower lithophysal rock and nearby talus piles on the southern end of Fran Ridge. The literature review showed that degradation in emplacement drifts and the resulting block size and bulking factor are influenced by existing fractures. The surface exposures and talus, therefore, may provide a link between fracture patterns and rubble fragment size and shape distributions.

Field work was performed to characterize surface exposures of the Ttptll zone on the southern end of Fran Ridge. A focused investigation on the size and shape distributions of rubble resulting from fractured lower lithophysal rock, along with detailed fracture data collection, provided an outcrop-scale rubble characterization for subsequent modeling efforts. Talus samples were collected for shape and size distribution analyses as well as laboratory experiments.

¹Exploratory Studies Facility is used frequently throughout this chapter; therefore, the acronym ESF will be used.

²Enhanced characterization of repository block is used frequently throughout this chapter; therefore, the acronym ECRB will be used.

³Topopah Spring welded Lower Lithophysal zone is used frequently throughout this chapter; therefore, the acronym Ttptll will be used.

B.2 FIELD INVESTIGATIONS

The south end of Fran Ridge at Yucca Mountain has outcrop exposures of the TSw Lower Lithophysal zone that are easily accessible (Figure B–1). Field conditions were sunny and dry. Three outcrop areas were delineated in the field, designated as Plot 1, Plot 2, and Plot 3. Plot 2 was further subdivided for rubble collection and characterization with subareas A, B, and C. Fracture data was collected from the three field outcrops. Data collection included fracture orientation, spacings, and tracelength (where it could be determined). Fracture orientation data was collected as strike, dip, and dip direction. Values were then converted to right-hand rule azimuth direction for subsequent analyses.



Figure B–1. Location Map of Fran Ridge Outcrop Sites

DRAFT

Talus was collected from directly beneath Plots 1 and 3; rubble was carefully collected directly from the outcrop and was not transported from adjacent areas (e.g., transported down slope from above the outcrop area). Known limitations to the field data include secondary alteration to the rubble (e.g., weathering and erosion effects). The smallest material in the talus piles of Plots 1 and 3 (i.e., fine-grained particles) were not included in the collection or analysis, because it was not possible to distinguish particles that originated from the outcrop from those introduced by eolian transport or other means. To minimize these effects, rubble from Plot 2 was removed directly from the outcrop with minimal force to provide the most “pristine” collection possible in the field. Staff attempted to collect all particle sizes from Plot 2 for subsequent laboratory experiments (see Appendix C), including fine-grained particles, although the fine material was not used in size distribution analysis. It was not possible to quantify the amount of fine-grained material that may have been transported into the outcrop or lost to erosion; this represents a limitation to the data collected at the outcrop. The percentage volume of fines in a rubble pile may influence the bulking factor (Peele, 1961).

Rubble data were recorded in the field with the following methodology: (i) clasts were photographed on a 2 by 2-cm [0.79 by 0.79-in] grid; (ii) the longest orthogonal dimensions (length, width, height) were measured; and (iii) all measurements were rounded to the nearest 0.5-cm [0.20-in] increment. Size limitations on the collection include truncations at the smallest and largest scale. The largest rock clasts collected were limited to the outcrop scale. The smallest clasts {~3–10 cm [1.18–3.94 in] in longest dimension} were too small to practically measure in the field. These clasts were binned by average size, laid out on the grid as close together as possible (representing the total length and width), and photographed as a group, with the largest and average heights recorded. Rubble particle volumes were averaged for these groups by calculating the overall length, width, and height of the collection and dividing by the number of clasts in the group.

Approximately 1,500 rubble clasts were photographed and measured during the field examination. Four 0.24-m³ [55-gal] drums of rubble were collected for further analyses (Figure B–2). Each drum contained a single rubble characterization site (e.g., sample drum #1 contains rubble collected and characterized from Plot 1). For Plot 2, only subareas A and B were collected. The largest clasts measured were wrapped separately on a pallet and tagged for sample identification.

Field observations indicate that the talus primarily resulted from degradation along existing outcrop fractures. Observations include a positive correlation between higher fracture intensity and smaller clast sizes. Also, fracture set orientations contributed to the shape of rock fragments (e.g., bladed or elongate). Field observations indicated most rock clasts were bladed, elongate, or platy in shape (Figure B–3). The least frequently encountered shape was cubic (i.e., equidimensional).

DRAFT



Figure B–2. Example Rubble Pile Collected From Plot 2 Outcrop at Fran Ridge

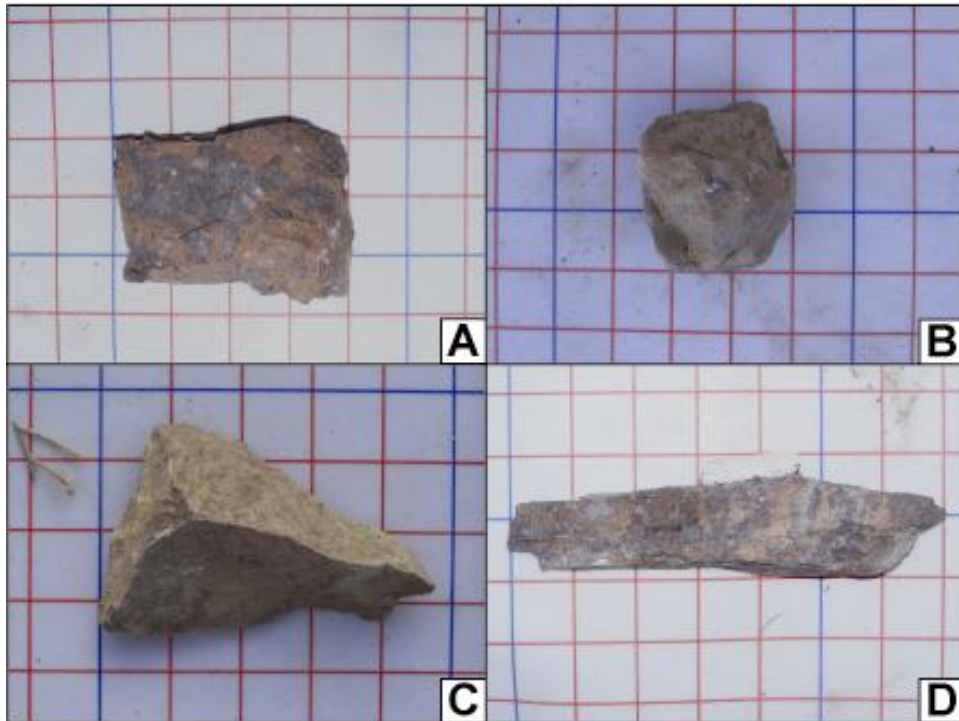


Figure B–3. Examples of Basic Rubble Shapes. (A) Platy, (B) Cubic, (C) Bladed, and (D) Elongate. Note That Background Grid Has 2 by 2-cm [0.79 by 0.79-in] Spacing.

DRAFT

B.3 FRACTURE CHARACTERIZATION

Three primary fracture sets were defined from the Fran Ridge outcrop data (Table B–1). Fracture data were analyzed with RockWare StereoStat® V. 1.4 for orientation and dispersion values to determine fracture sets. Set 1 is a north-northwest striking, steeply dipping set with an average strike and dip of 166°/73°. Mean spacing for Set 1 fractures is 7 cm [2.76 in]. Set 2 is an east-west striking, moderately dipping set with an average strike and dip of 101°/69°. Mean spacing for Set 2 fractures is 16 cm [6.30 in]. Set 3 is a subhorizontal fracture set with a mean strike and dip of 355°/15° and spacing of 9 cm [3.54 in].

A comparison of the Fran Ridge outcrop fractures (outcrop scale) in the TptplI to the fracture data Smart, et al. (2006) analyzed for the same zone recorded in the Detailed Line Survey in the ESF and ECRB (drift scale) shows similar fracture orientations (strike and dip) and spacing between these two sites (Figures B–4 to B–5). Both the outcrop scale and drift scale fracture analyses indicate three primary fracture sets: (i) a north-northeast striking, steeply dipping set; (ii) an east-west striking, steeply dipping set; and (iii) a subhorizontal set. The mean orientation of these three primary sets measured at Fran Ridge fall within the angular standard deviation (representing the degree of scatter) of the mean fracture set data observed in the ESF and ECRB. Fracture lengths between the two sites are not directly comparable (outcrop scale versus drift scale) as most fracture tracelengths at the outcrop were truncated because of the small exposures. A comparison of fracture spacing at the outcrop scale to the small-scale fracture data collected in the ECRB cross drift (cf., Table 1 this report; Smart, et al., 2006, Table 3-7) shows similar values for fracture spacing.

Some variations in fracture orientations and spacing are observed for each plot (Tables B–2 to B–4). Notably, Plot 3 differs from Plots 1 and 2 (and the ESF/ECRB fracture data) both in fracture set orientations and in fracture spacing. Fracture Set 2 (east-west striking, moderately dipping) was not found at Plot 3; instead, north-northwest striking, steeply dipping and north-northeast striking, steeply dipping fracture sets were observed. Plot 3 had smaller fracture spacing values overall. This variation in Plot 3 fracture data is likely due to its proximity to a mapped normal fault near the southeast end of Fran Ridge (Day, et al., 1998).

Table B–1. Summary of Fran Ridge Fracture Data Collected at All Plots

Fracture Set	Mean Orientation	Angular Standard Deviation	Fisher Dispersion Coefficient*	True Spacing (cm) [in]	
				Mean	Median
Fran Ridge (this report)					
Set 1	129°/72°	64°	13.3	7.3 [2.87]	6.2 [2.44]
Set 2	101°/69°	17°	21.8	16.3 [6.42]	12.5 [4.92]
Set 3	355°/15°	12°	42.4	9.1 [3.58]	8.5 [3.35]
Table 3-7†					
Set 1	134°/82°	45°	3.3	10.8 [4.25]	3 [1.18]
Set 2	079°/82°	21°	14.6	24 [9.45]	12 [4.72]
Set 3	313°/04°	12°	47.4	10 [3.94]	6 [2.36]
*The Fisher dispersion coefficient (also referred to as the concentration parameter) is a measure of the degree to which spherical data are concentrated around the mean (N.I. Fisher, T. Lewis, and B.J.J. Embleton. "Statistical Analysis of Spherical Data." Cambridge, United Kingdom: Cambridge University Press. 1993). Larger values of the Fisher dispersion coefficient indicate tighter clustering (i.e., less dispersion). †Smart, K.J., D.Y. Wyrick, P.S. Landis, and D.J. Waiting. "Summary and Analysis of Subsurface Fracture Data From the Topopah Spring Tuff Upper Lithophysal, Middle Nonlithophysal, Lower Lithophysal, and Lower Nonlithophysal Zones at Yucca Mountain, Nevada." CNWRA 2005-04. ML060660009. San Antonio, Texas: Center for Nuclear Waste Regulatory Analyses 2006.					

DRAFT

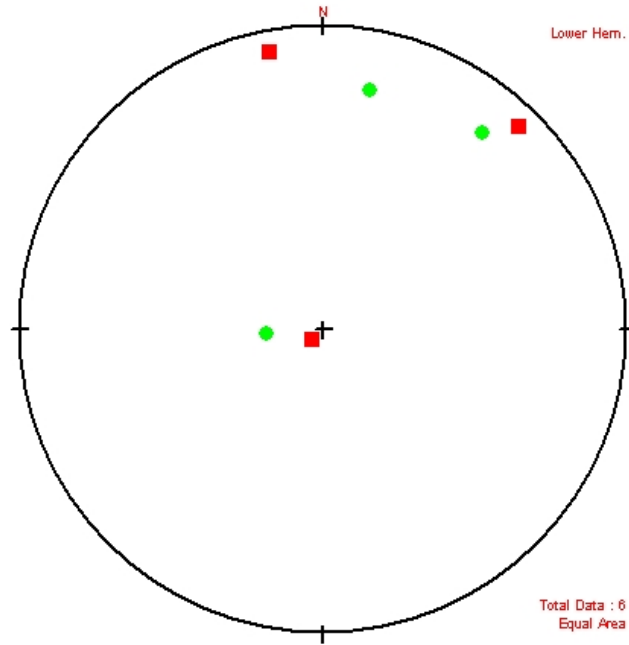


Figure B-4. Equal-Area Stereonet Plot of Poles to Fracture Planes From Fracture Orientation Data Collected at Fran Ridge Outcrop (Green Circles) and the ESF/ECRB Detailed Line Survey Small-Scale Fracture Data (Red Circles; Smart, et al., 2006, Figure 3-10).

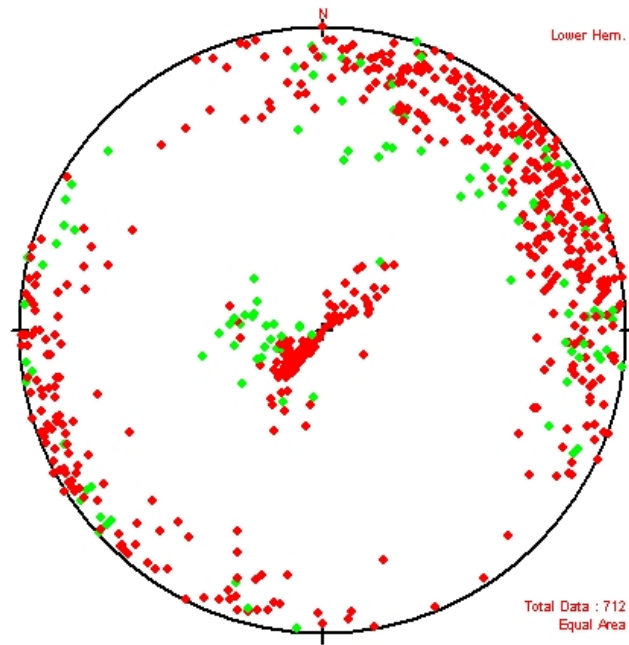


Figure B-5. Equal-Area Stereonet Plot of Poles to the Mean Fracture Set Planes from Table B-1.

DRAFT

DRAFT

Table B-2. Summary of Fran Ridge Fracture Data Collected at Plot 1		
Fracture Set	Mean Orientation	True Spacing (cm) [in] Mean
Set 1	170°/71°	10.2 [4.02]
Set 2	097°/24°	12.1 [4.76]
Set 3	007°/24°	15.4 [6.06]

Table B-3. Summary of Fran Ridge Fracture Data Collected at Plot 2		
Fracture Set	Mean Orientation	True Spacing (cm) [in] Mean
Set 1	164°/73°	7.6 [2.99]
Set 2	102°/69°	17.2 [6.77]
Set 3	349°/17°	8.4 [3.31]

Table B-4. Summary of Fran Ridge Fracture Data Collected at Plot 3		
Fracture Set	Mean Orientation	True Spacing (cm) [in] Mean
Set 1	172°/76°	4.3 [1.69]
Set 2	—	—
Set 3	353°/13°	6.8 [2.68]
Set 4	332°/85°	3.64 [1.43]
Set 5	022°/83°	2.75 [1.08]

DRAFT

B.4 RUBBLE CHARACTERIZATION

B.4.1 Clast Shape Distribution

The literature reviewed shows that rubble clast shape influences bulking factor (Pappas and Mark, 1993). To characterize the shape distribution of rubble, a classification system that captures the wide range of clast shape is required. A literature search of the types of clast shape classifications systems indicates that a modified Sneed and Folk (1958) organization that includes shape ranges from cubic (equidimensional), platy (tabular), bladed, and elongate (rod) is suitable for these analyses (Sneed and Folk, 1958; Graham and Midgley, 2000). Sneed and Folk (1958) diagrams, employing ratios of the three orthogonal particle axes, have been advocated as the most appropriate method for unbiased presentation of primary particle shape data. A Sneed and Folk (1958) diagram is scaled such that independent (although related) variables can be plotted for one axis without necessarily affecting the other two. For any given particle, the values of the three axes (length, width, and height) are independent, except that, by definition, $Length \geq Width \geq Height$. This type of triangular diagram differs from traditional ternary plots where the three variables plotted represent relative proportions of a whole (i.e., a decrease in one variable will produce increases in one or both of the other variables). The four major shape classifications (cubic, platy, elongate, and bladed) are illustrated in Figure B-6 to show the general block shapes and their locations on the chart.

For the major classifications, subdivisions are grouped such that cubic = all cubic values; platy = cubic-platy + platy + very platy; bladed = cubic-bladed + bladed + very bladed; elongate = cubic-elongate + elongate + very elongate. The major shape classifications could be grouped slightly differently (e.g., cubic could include cubic + cubic platy + cubic elongate + cubic bladed). Both values are provided in this report. The most common rubble shape was bladed fragments, representing 39–48 percent of all rubble clasts; elongate shapes represented 26-31 percent of all rubble. These two primary shapes combined comprised 65–79 percent of the outcrop rubble measured. Clast shape data for all the Fran Ridge outcrop samples are illustrated in Figures B-7 to B-10.

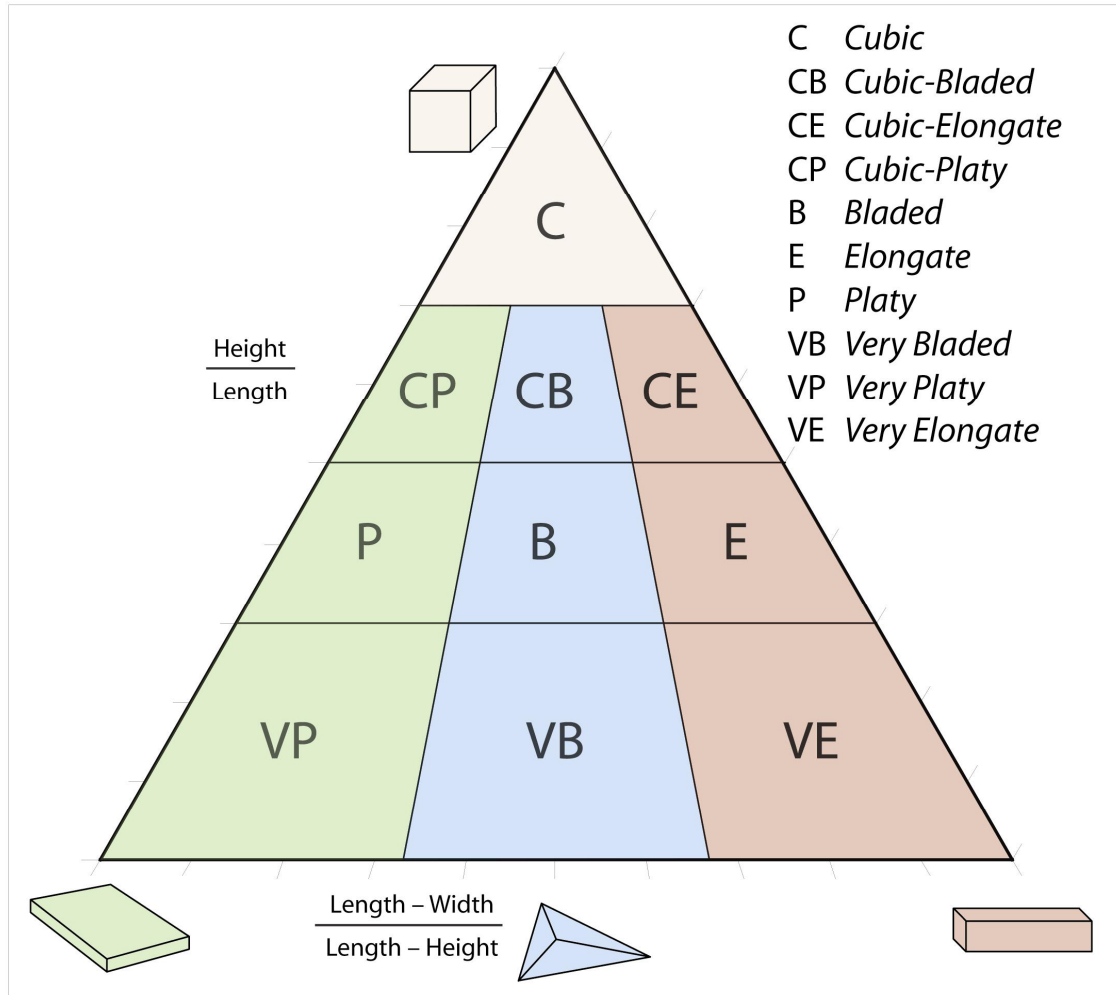


Figure B–6. A Modified Sneed and Folk Diagram Representation of Particle Shape (Sneed and Folk, 1958; Graham and Midgley, 2000). Sneed and Folk Diagrams Employ Ratios of the Three Orthogonal Particle Axes To Present Primary Particle Shape Data.

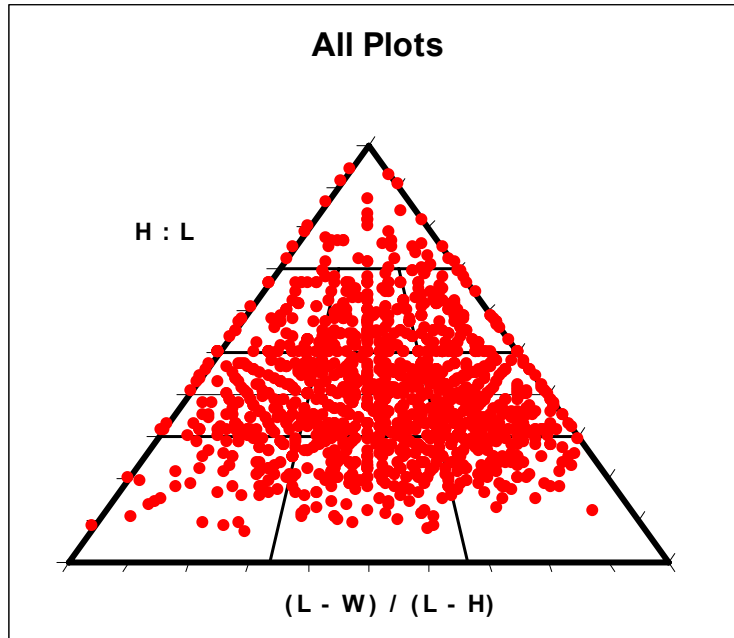


Figure B-7. Modified Sneed and Folk Diagram of All Rubble Shape Data

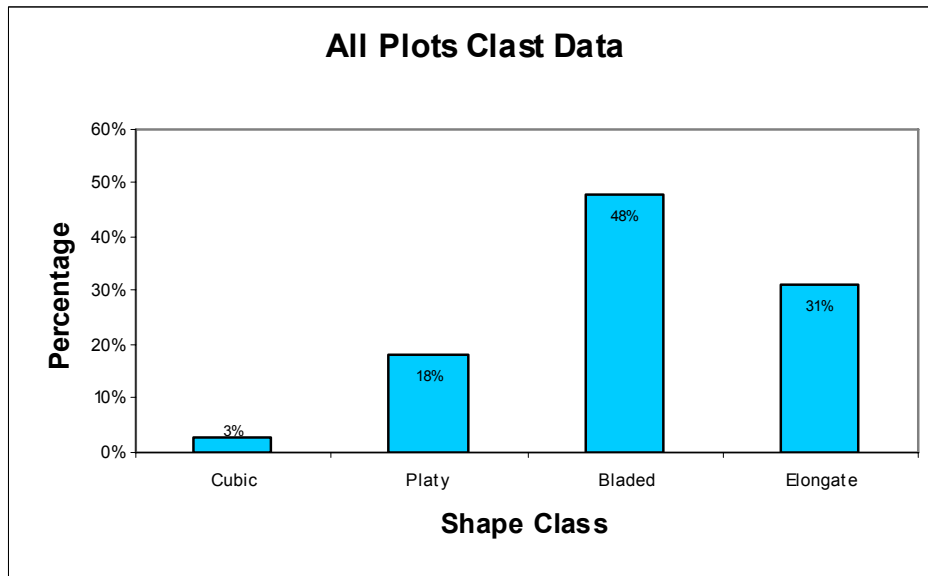


Figure B-8. Rubble Shape Major Classification by Percentage for All Rubble Shape data. In This Chart, Cubic = Cubic; Platy = Cubic-Platy + Platy + Very Platy; Bladed = Cubic-Bladed + Bladed + Very Bladed; Elongate = Cubic-Elongate + Elongate + Very Elongate.

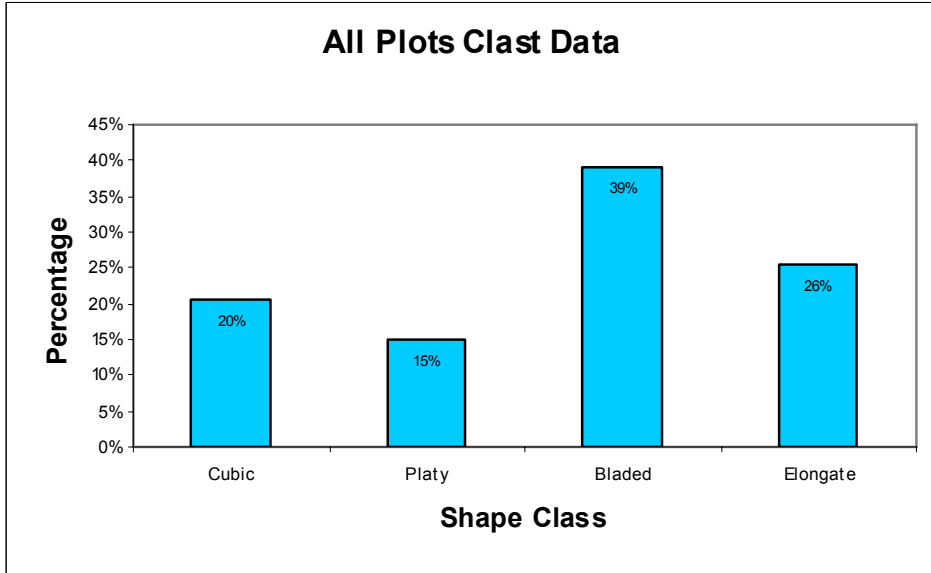


Figure B-9. Rubble Shape Major Classification by Percentage for All Rubble Shape Data. In This Chart, Cubic = Cubic + Cubic Platy + Cubic Elongate + Cubic Bladed; Platy = Platy + Very Platy; Bladed = Bladed + Very Bladed; Elongate = Elongate + Very Elongate.

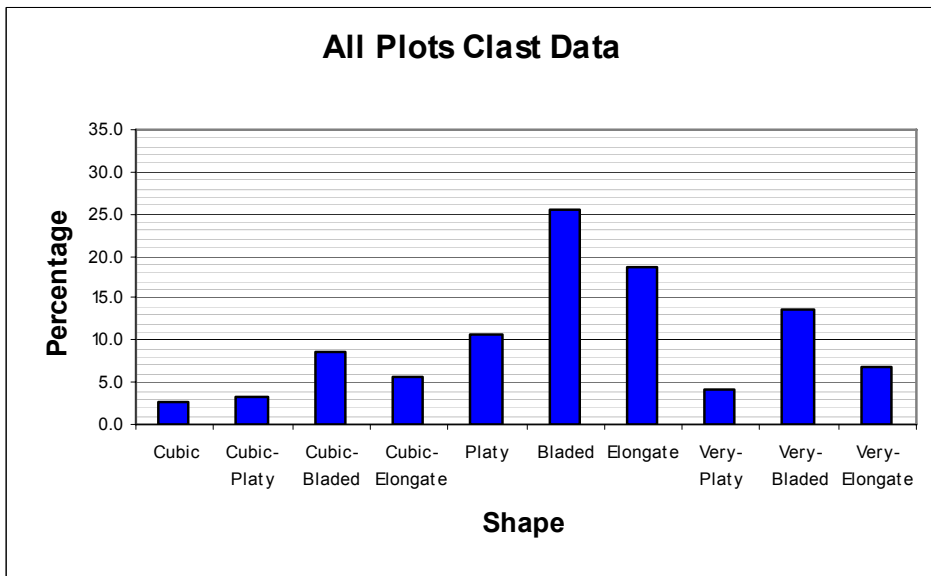


Figure B-10. Rubble Shape Classification Detail by Percentage for All Rubble Shape Data

DRAFT

Plot 1A

Plot 1A rubble was collected from the talus pile located directly beneath the outcrop (Figure B-11). Rubble fragments from this location are primarily bladed and elongate in shape (Figures B-12 to B-15).



Figure B-11. Field Photograph of Talus Pile Location for Plot 1A

DRAFT

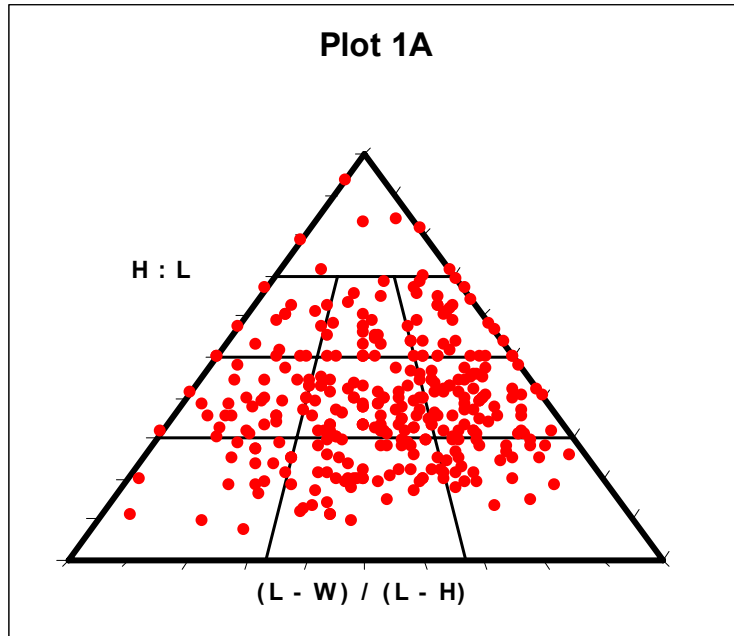


Figure B-12. Modified Sneed-Folk Diagram of Plot 1A Rubble Shape Data

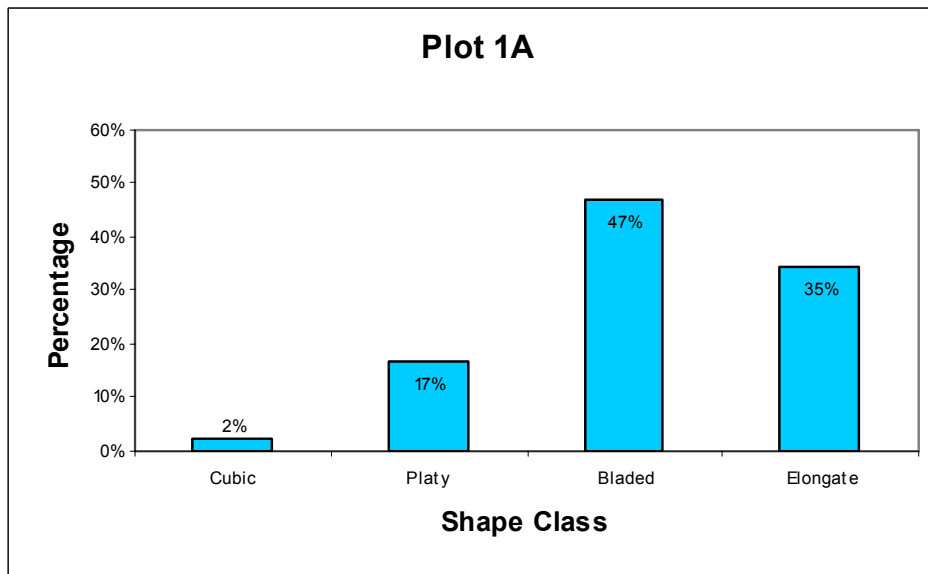


Figure B-13. Rubble Shape Major Classification by Percentage for Plot 1A Rubble Shape Data. In This Chart, Cubic = Cubic; Platy = Cubic-Platy + Platy + Very Platy; Bladed = Cubic-Bladed + Bladed + Very Bladed; Elongate = Cubic-Elongate + Elongate + Very Elongate.

DRAFT

DRAFT

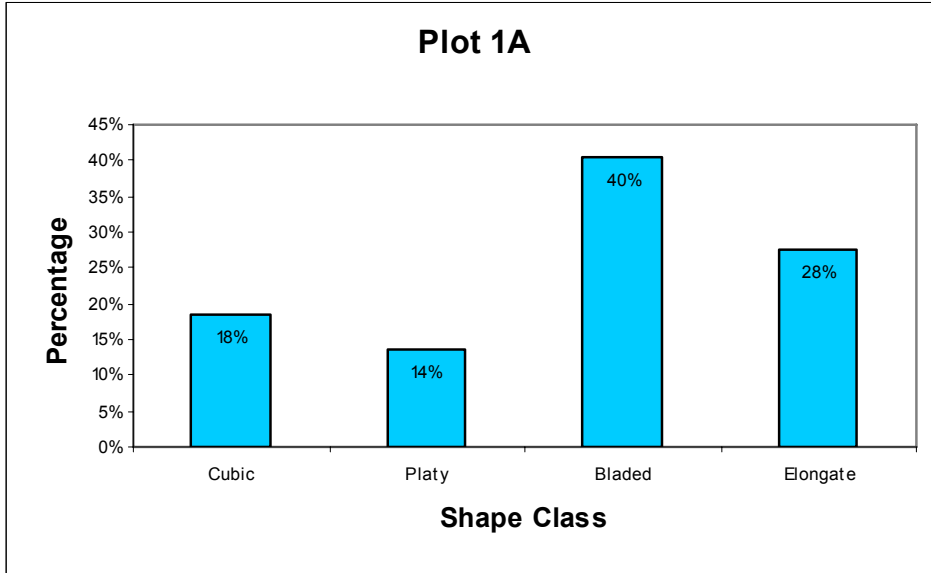


Figure B-14. Rubble Shape Major Classification by Percentage for Plot 1A Rubble Shape Data. In This Chart, Cubic = Cubic + Cubic Platy + Cubic Elongate + Cubic Bladed; Platy = Platy + Very Platy; Bladed = Bladed + Very Bladed; Elongate = Elongate + Very Elongate.

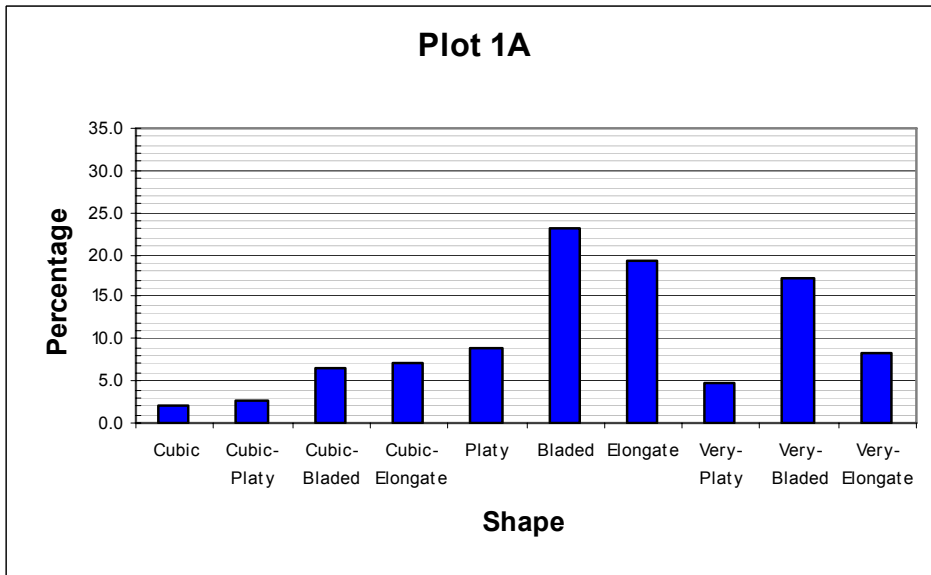


Figure B-15. Rubble Shape Classification Detail by Percentage for Plot 1A Rubble Shape Data